7-11-2015

A Resonant Based Test Methodology for Capacitive MEMs

Ali Dianat
University of Windsor

Recommended Citation
Dianat, Ali, "A Resonant Based Test Methodology for Capacitive MEMs" (2015). *Electronic Theses and Dissertations.* Paper 5297.

A Resonant Based Test Methodology for Capacitive MEMs

By

Ali Dianat

A Thesis

Submitted to the Faculty of Graduate Studies
through the Department of **Electrical and Computer Engineering**
in Partial Fulfillment of the Requirements for
the Degree of **Master of Applied Science**
at the University of Windsor

Windsor, Ontario, Canada

2015

A Resonant Based Test Methodology for Capacitive MEMS

By

Ali Dianat

APPROVED BY:

Dr. A. Azab
Mechanical, Automotive & Materials Engineering

Dr. K. Tepe
Electrical & Computer Engineering

Dr. R. Rashidzadeh, Co-Advisor
Electrical & Computer Engineering

Dr. R. Muscedere, Co-Advisor

Electrical & Computer Engineering

April. 14/2015

Declaration of Co-Authorship and Previous Publications

I. Co-Authorship Declaration

I hereby declare that this thesis incorporates the outcome of a research in collaboration with and under the supervision of Dr. Rashid Rashidzadeh and Dr. Roberto Muscedere with the review and revision being provided by Dr. Rashid Rashidzadeh.

The collaboration is covered in chapter 3, 4 and 5 of the thesis. In all cases, the primary contributions were performed by the author Mr. Ali Dianat and the co-author Mr. Ali Attaran through supervision of Dr. Rashid Rashidzadeh and Dr. Roberto Muscedere.

I am aware of the University of Windsor Senate Policy on Authorship and I certify that I have properly acknowledged the contribution of other researchers to my thesis, and have obtained written permission from each of the co-author(s) to include the above material(s) in my thesis. I certify that, with the above qualification, this thesis, and the research to which it refers, is the product of my own work.

II. Declaration of Previous Publication

This thesis includes one original paper that has been previously published, one original paper that has been accepted for publication in peer reviewed conferences, and one journal paper that is submitted as follows:

Thesis Chapter	**Publication title/full citation**	**Publication status**
Chapter 3	A. Dianat, A. Attaran, R. Rashidzadeh, and R. Muscedere , "Resonant-Based Test Method for Capacitive MEMS Devices", IEEE International Conference on Electronics Circuit and Systems (ICECS), December7-10, 2014,Marseille, France	Published
Chapter 4	A. Dianat, A. Attaran, R. Rashidzadeh, "Test Method for Capacitive MEMS Devices Utilizing Pierce Oscillator", IEEE International Symposium on Circuits and Systems (ISCAS), May24-27, 2015, Lisbon, Portugal	Accepted
Chapter 5	A. Dianat, A. Attaran, R. Rashidzadeh, "Self-ResonationTest Methodology for Capacitive MEMS", special issue of Analog Integrated Circuits and Signal Processing (AICSP) journal edited by Springer	Submitted

I certify that I have obtained a written permission from the copyright owner(s) to include the above published material(s) in my thesis. I certify that the above material describes work completed during my registration as graduate student at the University of Windsor.

I certify that, to the best of my knowledge, my thesis does not infringe upon anyone's copyright nor violate any proprietary rights and that any ideas, techniques, quotations, or any other material from the work of other people included in my thesis, published or otherwise, are fully acknowledged in accordance with the standard referencing practices. Furthermore, to the extent that I have included copyrighted material that surpasses the bounds of fair dealing within the meaning of the Canada Copyright Act, I certify that I have obtained a written permission from the copyright owner(s) to include such material(s) in my thesis and have included copies of such copyright clearances to my appendix.

I declare that this is a true copy of my thesis, including any final revisions, as approved by my thesis committee and the Graduate Studies office, and that this thesis has not been submitted for a higher degree to any other University or Institution.

ABSTRACT

This work presents a test method for capacitive Micro-Electro-Mechanical Systems (MEMS). A major class of MEMS sensors operate based on the principle of capacitance variation.The proposed test method in this work utilizes a resonant circuit to detect structural defects of capacitive MEMS sensors. It is shown that a small variation of MEMS capacitance due to a defect alters the resonance frequency considerably. It is also shown that the variation of the output amplitude can be observed for fault detection if an inductor with a high quality factor is employed in the test circuit. Mathematical approach is taken and verified to prove the validity of this work. The effects of structural defects such as short, broken and missing fingers of the MEMS comb-drive on the equivalent circuit models have been determined through frequency domain simulations. Simulation results and experimental measurements using an implemented MEMS comb drive indicate that the proposed method can detect common faults such as missing, broken and short fingers.

DEDICATION

I would like to dedicate my work to my family, relatives and friends. A special feeling of gratitude to my loving parents, Dr. Mohammad Dianat and Mrs. Farahnaz Toofani whose words and their existence are the source of encouragement that inspires me throughout my life. Thank you mom, thank you dad for always being there for me and have taught me the meaning of love and caring. No matter how old I am I always need you and your love.

I dedicate my work to my lovely wife, Zainab for her exceptional support and love. Thank you so much Zaza for being engaged with all struggles and discomfort that I may given you during my studies, your practical and emotional support as a role of wife and mother who was also a full-time student is truly appreciated and your unique help to complete my work will never be forgotten. Thank you for everything you do for me. I love you forever.

I dedicate this work to my beautiful angel, my lovely daughter Sarah Dianat who always brings happiness and joy to my life and her unique presence has always motivated me to look forward to complete my studies and my work. I cherish all the wonderful moments I spend with you Bishi and I always thank god for having you in my life.

I also wish to give my special thanks to my best friend and my colleague, Dr. Ali Attaran for his support and perfect assistance by providing me with many constructive guidance, directions and feedbacks throughout my program and take part in my publications as well and help me to master in my area of studying and being my cheer leader.

ACKNOWLEDGEMENTS

I would like to give special thanks to my supervisors, Dr. Rashid Rashidzadeh and Dr. Roberto Muscedere, for their exceptional support, encouragement and valuable suggestions. I really benefited a lot from discussions with them during my research work. Their creativeness, diligence and passion towards research inspired me a lot when I had a hard time in my research. I also would like to thank Dr. Kemal Tepe and Dr. AhmedAzab for their valuable comments.

TABLE OF CONTENTS

DECLARATION OF CO-AUTHORSHIP AND PREVIOUS PUBLICATIONS iii

ABSTRACT vi

DEDICATION vii

ACKNOWLEDGEMENTS viii

LIST OF ABBREVIATIONS/SYMBOLS xi

Chapter 1Introduction and Background 1

- 1.1 Micro-Electro Mechanical Systems(MEMS) 1
  - 1.1.1 A brief introduction to Micro-Electro Mechanical Systems 1
  - 1.1.2 MEMS applications 2
  - 1.1.3 Microsystems historical background 3
  - 1.1.4 MEMS operational zone 5
  - 1.1.5 MEMS market share 5
- 1.2Capacitive Micro-Electro Mechanical Systems(MEMS) 7
- 1.3Implementation and modeling of micro-electro mechanical systems 8
  - 1.3.1CAD Tools 8
  - 1.3.2Coventorware CAD tool 8

1.3.3Agilent ADS CAD tool..8

Chapter 2Micro-Electro Mechanical Systems fabrication process..............................9

2.1 MEMS Material 9

2.2 Cost of a typical MEMS Devices...17

2.3 Microsystems General Test Approach 18

2.4MEMS Test Solution Proposed in The Literature 19

Chapter 3 Resonant-Based Test Method for MEMS Devices...................................22

Chapter 4 Test Method for Capacitive MEMS Using Pierce Oscillator....................33

Chapter 5 Self-Resonation Test Methodology for Capoacitive MEMS.....................43

Chapter 6 Conclusion 68

References 69

VITA AUCTORIS...75

LIST OF ABBREVIATIONS/SYMBOLS

Abbreviations:

ABBREVIATIONS	DESCRIPTION
MEMS	Micro-Elecrto Mechanical Systems
DUT	Device Under Test
PVD	Physical Vapour Deposition
CVD	Chemical Vapour Deposition
LPCVD	Low Pressure Chemical Vapour Deposition
PECVD	Plasma Enhanced Chemical Vapour Deposition
ATE	Automatic Test Equipment
FEA	Finite Element Analysis
IC	Integrated Circuit
CMOS	Complementary Metal–Oxide–Semiconductor
CAD	Computer-Aided Design
EDA	Electronic design automation
ADS	Advanced Design System

Chapter 1

Introduction and Background

1.1 Micro-Electro Mechanical Systems

1.1.1 A brief introduction to Micro-Electro-Mechanical Systems

Micro-electro mechanical systems (MEMS) is a technology to fabricate small devices that can be integrated with microelectronic circuits. MEMS technology covers multi-disciplinary area and it includes many fields of applications including optical devices, thermal, fluidic and magnetic. MEMS structure can vary from a simple structure with no moving element to a very complex system with multiple moving elements. MEMS devices are able to convert energy from one domain to another [1].

MEMS technology can be utilized in several domains. For instance design of micro-sensors, microstructures and micro-actuators are performed through MEMS technology. Figure 1.1[2] demonstrates different MEMS sectors with respect to their applications.

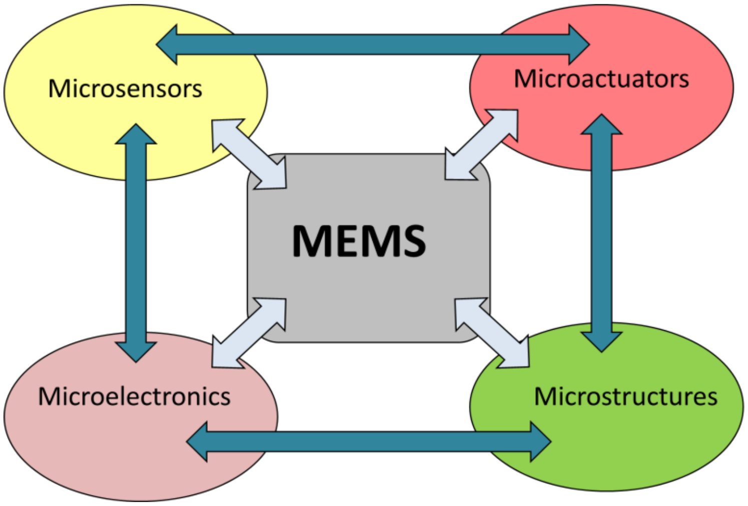

Fig. 1.1 MEMS sectors with respect to their application on a single integrated chip [2].

1.1.2 MEMS application

MEMS devices have many applications in different areas such as automotives, medical, industrial, avionics, optical communications and electronics. For example pressure sensors are utilized vastly in automotive industry such as tire pressure monitoring systems, crash detection for airbags and oil pressure sensing [3]. In medical sector they broadly used as disposable sensors to monitor blood pressure of patients requiring intensive care. To name other applications we can mention shock and motion detection sensors, image stabilizers in cameras, embedded microphones and screen rotation features in cell phones.

1.1.3 Microsystems historical background

The number of transistors in Integrated Circuits (IC) has doubled every 18 months since 1970 as predicted by Moor's law. Figure 1.2[4] presents the plot of microprocessor transistor counts with respect to date of their introduction to the market.

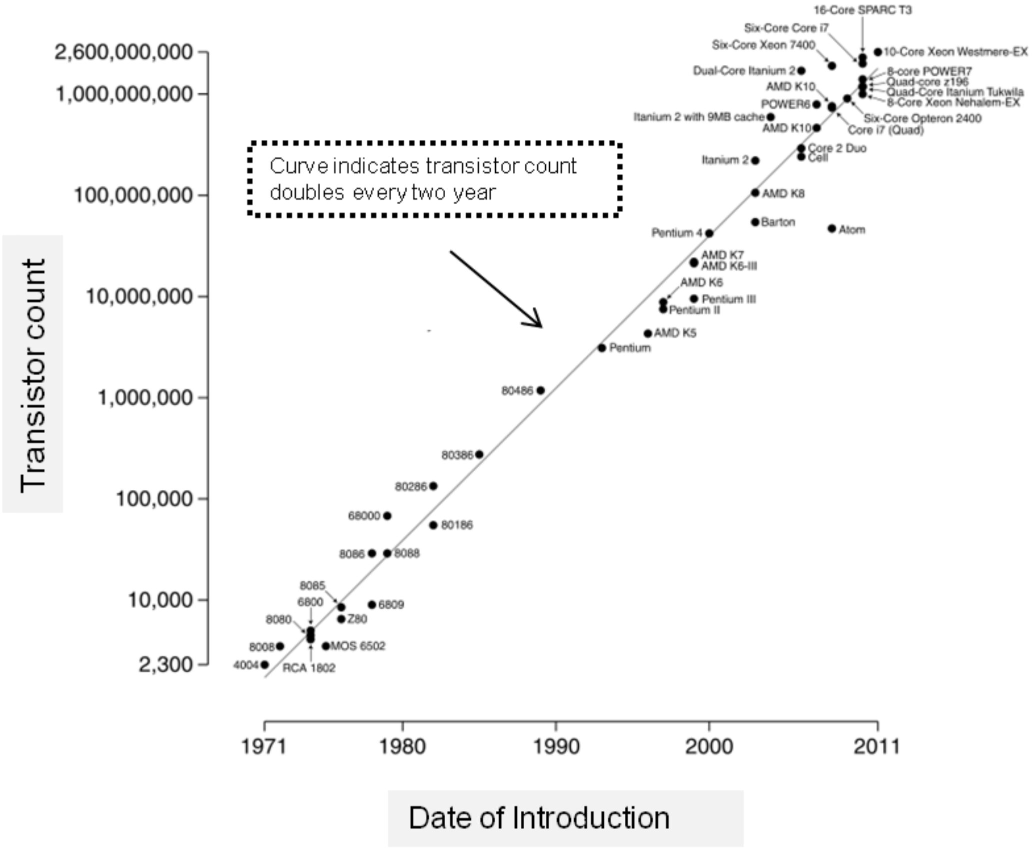

Figure 1.2 CPU transistor counts from 1971 to 2011 following Moor's law [4]

It can be observed that approximately every 18 months the transistor count doubles. Currently in commercially available CPUs there are over 4 billion transistors which provide a considerable processing power.

In 1958, Jack Kilby (inventor of IC) introduced his first integrated circuit at Texas Instrument in Dallas which was a revolution in electronic circuits. This integrated circuit contained a single transistor, three resistors and a capacitor on a chip of germanium in a millimeter scale. This was a significant starting point to open a gate for researchers todevelop complex ICs and attempt to fabricate circuits in a much smaller area. Table 1.1demonstrates the historical perspective of micro systems [5].

Year	**Name of Invention/Discovery**
1824	Silicon discovered (Berzelius)
1948	First transistor (Bardeen, Brattain, Shockley, Bell Lab)
1954	Piezoresistive effect in Germanium and Silicon discovered
1958	First integrated circuit (Kilby, TI)
1961	First silicon pressure sensor (Kulite)
1964	First batch fabricated MEMS (Nathanson)
1967	Surface micromachining invented (Nathanson)
1970	First silicon accelerometer (Kulite)
1971	First single chip microprocessor (Intel)
1977	First capacitive pressure sensor (Stanford)
1984	First poly-silicon MEMS device (Howe, Muller)
1989	Lateral comb drive (UC Berkeley)
1992	Diffraction grating light modulator (Stanford)

1999	First optical network switch (Lucent technologies)
2000	Micro gas turbine engine (MIT)
2000s	Increasing number of MEMS devices and their applications

Table 1.1 Historical perspectives of micro systems

1.1.4 MEMS operational zone

MEMS devices are able to sense, receive, control, transmit and actuate in micro scale. Figure 1.3 displays the block diagram of MEMS operational zone and their application [7].

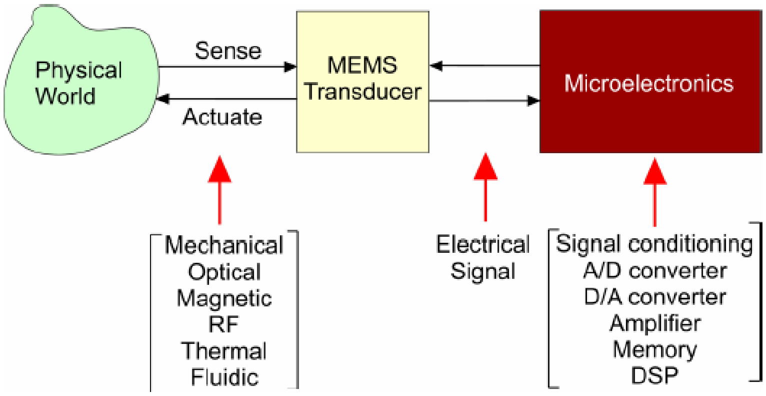

Figure 1.3 Typical MEMS operational zone [7].

1.1.5 MEMS market share

MEMS industry has been growing dramatically since 2001 and has an estimated of $10 billion market with the projected annual growth rate of 10-20%.Silicon pressure sensor alone is a billion-dollar industry [6]. Figure 1.4[7] displays the estimated percentage of the market share projection for different types of MEMS devices in 2007. The overall prediction of worldwide MEMS revenue forecast per application is graphically demonstrated in figure 1.5.

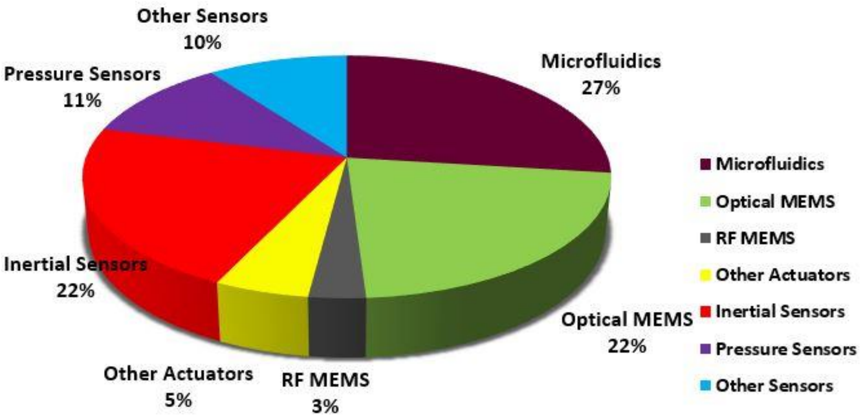

Figure 1.4 Typical MEMS operational zone [7].

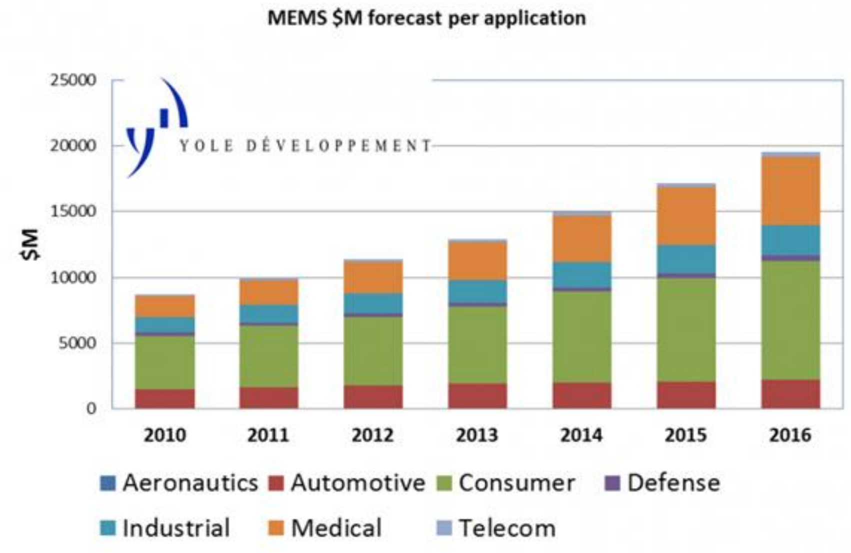

Figure 1.5 Worldwide revenue forecast for MEMS from 2010 to 2016 [8].

It can be observed that there is a great potential in the MEMS and Microsystems industry as manufacturers invest billions of dollars in these technologies. There are lots of advantages in MEMS technology that makes it very attractive. As the fabricated devices scale down, the power consumption per function drops and the speed increases which eventually lowers the costs of Microsystems.

1.2 Capacitive Micro-Electro Mechanical Systems

Capacitive MEMS devices contain energy-storage element which it can be modeled as typical capacitor. This capacitor can be defined in terms of a relationship between displacement and effort. Capacitors are associated with potential energy which means whenever it has a non-zero effort there is some stored energy in the capacitor. A simple example of capacitive MEMS devices as shown in figure 1.6[9] is MEMS microphone which operates based on the principle of capacitance sensing.

Figure 1.6 CMOS-based Capacitive MEMS microphone introduced by Akustica [9].

1.3 Implementation and modeling of micro-electro mechanical systems

1.3.1CAD Tools

Capacitive MEMS devices can be modeled by various 3-D finite element analysis (FEA) CAD tools such as Intellisuite, Coventorware, MEMSCAP, FEMLAB, ANSYS, ALGOR, and MEMSPRO. MATLAB can also be used for analytical modeling.

1.3.2Coventorware CAD tool

Coventorware is an integrated suite of design and simulation software that provides the accuracy and capacity to address real-world MEMS designs.

1.3.3Agilent ADS CAD tool

Advanced design system (ADS) is one of the world’s leading electronic design automation (EDA) software. ADS in this work mainly is used to generate the layout of the design and observe the S-parameters.

Chapter 2

Micro-Electro Mechanical Systems fabrication process

2.1 MEMS material

Micro fabrication is based on planar technologies which involve implementing MEMS components and electronic devices on a substrate that originally are in the form of flat wafers. Microelectronics industry invested huge amounts of dollars to develop wafer based process technologies [1].MEMS fabrication process is similar to the conventional VLSI technology where three dimensional microstructures are fabricated on a microchip [1]. In other words, MEMS is a logical evolution of the VLSI technology which adds new dimensions to microchips and introduces new functionalities to microelectronic devices. There are two main methods for micro fabrication (a) Wafer-level processes (including wafer bonding) and (b) pattern transfer (isotropic and anisotropic etching).

First step in MEMS fabrication process is the substrate material selection. This includes single-crystal quartz, single-crystal silicon, glass and fused quartz. Recently special attention is also given to gallium arsenide due to their variety of application in optoelectronic device fabrication.

In general, silicon is introduced as a semiconductor that can be doped to act like a conductor or used as an insulator. One of the advantages of silicon is its great stability against temperature as it can maintain its property as semiconductor at high temperatures.

Due to many advantages in using silicon in MEMS technology, sometimes it is also referred as second silicon revolution. Single-crystal silicon wafers are dominantly utilized as a substrate to initiate the fabrication process. They are classified by the pattern orientation and most silicon crystals are grown utilizing Czochralski (CZ) method. Another method for growing silicon crystal is the float zone (FZ) which has higher purity compared to the CZ method.

Prior to using a wafer as a substrate for fabrication, it must be cleaned to avoid any problem that may affect the fabrication process. The standard set of wafer cleaning is called RCA by removing all organic coatings through a strong oxidant [1]. The RCA cleaning should be carried out prior to high-temperature steps such as oxidation, diffusion, chemical or vapour deposition [1]. Figure 2.1[7] presents the block diagram of a simplified MEMS fabrication process. After wafer level, deposition is carried out and followed by lithography and etching.

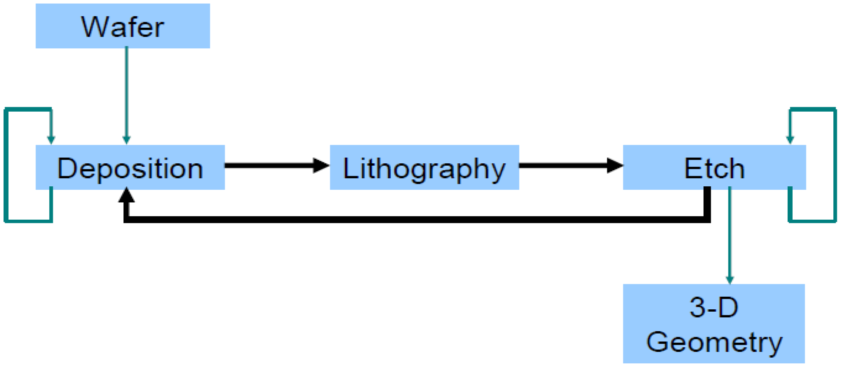

Figure 2.1 MEMS fabrication process [7].

Many microelectronics fabrications include deposition processes that relatively depend on the designer what deposition method to be undertaken. Most common deposition process is based on TFD (Thin Film Deposition) that is also referred to as additive process. Physical vapour deposition (PVD) and chemical vapour deposition (CVD) are also used in deposition methods. Practically, most commercially significant CVD processes are low-pressured; hence the process is sometimes called low pressure chemical vapour deposition (LPCVD). If deposition rate needs to be more enhanced then PECVD (plasma enhanced chemical vapour deposition) is used which occurs in glow-discharge plasma [1]. Other additive processes are available for MEMS fabrication which is relatively expensive such as electro-deposition, lift off and spin casting methods.

After deposition process, optical lithography is performed. This process is pretty much similar to the photographic process of printing from a negative image on a photosensitive paper.

In order to create a pattern, a photo-mask is used which transfers a set of transparent and opaque region. Then ultraviolet light is emitted through the photo-mask onto the wafer and this will change the chemical properties of the unprotected portion exposed to the light [1]. Figure 2.2 [7] displays the block diagram of the photolithography process for MEMS fabrication.

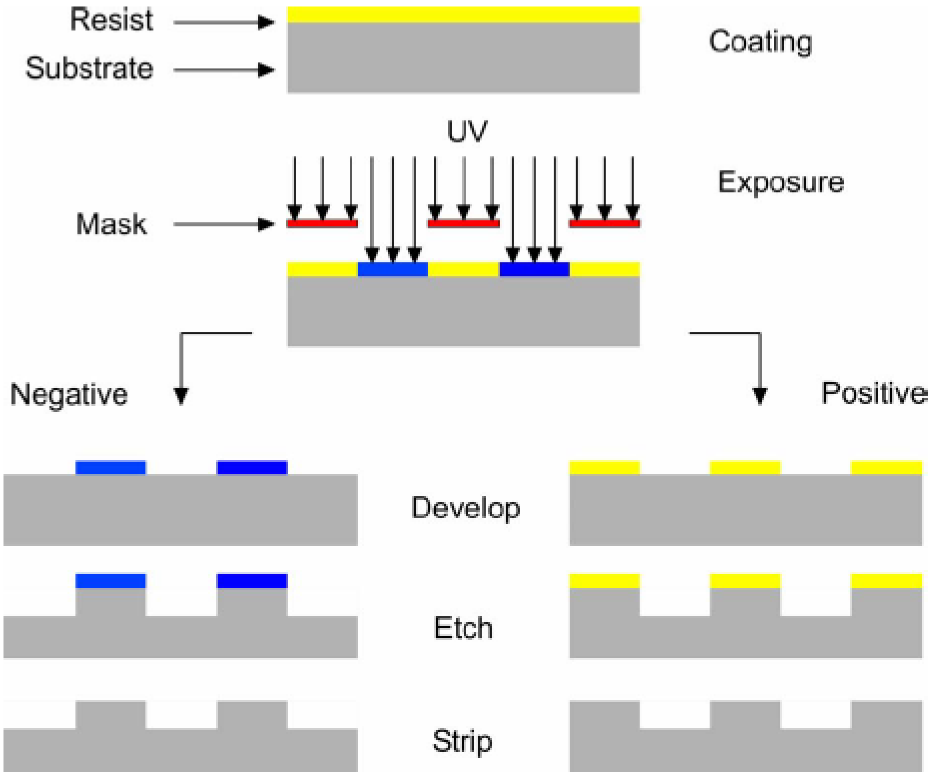

Figure 2.2 Photolithography process [7].

On the opposite side of deposition process, etching process is performed which is also called subtractive process. It basically refers to the process of removing the deposited layer through the patterned mask and the openings created in the previous stages. There are two main etching techniques utilized by the industry, known as Wet and Dry etching.

The conventional approach in etching process is to immerse the patterned substrate in a suitable chemical liquid that reacts with the exposed region of the substrate and leaves the unexposed region intact [1].There are many factors that can affect the rate and shape of etching features such as type of substrate, material of the etchant, and selection of masking layer and how tight the adhesion to the substrate is. The temperature is also extremely important in order to control the reaction rates.

As mentioned, there are two main techniques of etching called Wet and Dry etching. The Wet etching is mainly isotropic which means the orientation of the substrate will not be affected by the rate of material removal in printing from a negative on the etching process and they are independent of each other. Therefore the etching occurs in all direction. Figure 2.3 [7] demonstrates the concept of isotropic etching.

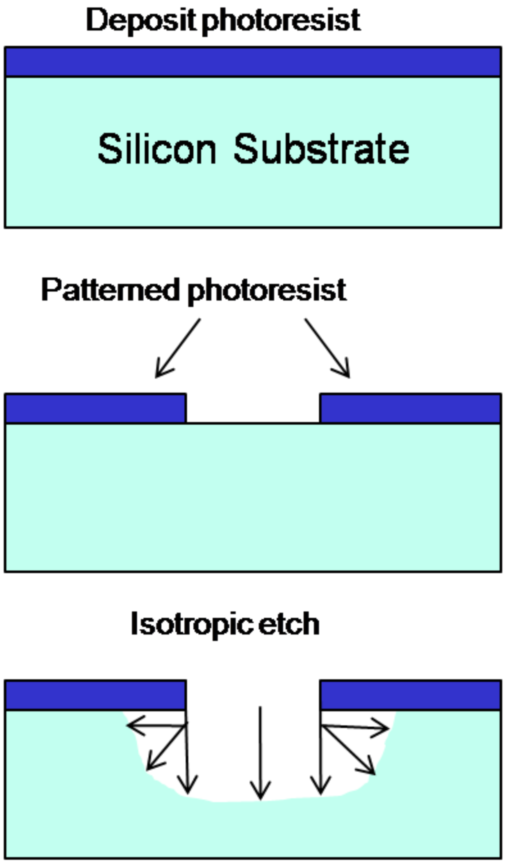

Figure 2.3 isotropic etching [7].

It can be seen that the patterned photo-resist is undercut and lateral etching is formed at about the same rate as vertical etching. This is due to isotropic properties of the etchant.

Table 2.1 illustrates various materials that can be etched with wet etchant [1].

Material	**Etchant**
Thermal or CVD silicon dioxide	Buffered hydrofluoric acid
Polysilicon	KOH or ethylene diamine
Silicon nitride	Hot phosphoric acid
Aluminum	PAN (Phosphoric, acetic, nitric acids)
Copper	Ferric Chloride
Gold	Ammonium iodide/iodine alcohol

Table 2.1 wet etchant selection

There are complete etchant database including selectivity and etch rates in [10, 11]. In contrast with isotropic etching, there is anisotropic etching process in which the etch rate depends on the orientation of the substrate. For example potassium hydroxide (KOH), ethylene diamine pyrochatecol (EDP) and tetramethyl ammonium hydroxide (TmAH) exhibit high dependency on the orientation of the substrate for etch characteristics in silicon [12]. Similar orientation-dependent effect is observed from hydrofluoric acid for single crystal quartz etching [13].

Similar to Wet etching, Dry etching is also classified as isotropic etching and anisotropic etching with the same concept. In Dry etching process chemically reactive vapours are highly effective etchant [1]. The most commercially important vapour etchant in micromachining technique is the gas of xenon difluoride (XeF_2) which for silicon is a highly selective vapour etchant [14].

There are also some other etch gases for dry etching of different material that are illustrated in table 2.2[15, 16, 17].

Etch gas	Material to be etched
$\boldsymbol{CF_4, SF_6}$	Silicon or poly-silicon
$\boldsymbol{CF_4,/O_2}$	Silicon nitride
$\boldsymbol{CF_4/H_2}$	Silicon dioxide
$\boldsymbol{O_2, O_2/CF_4, O_2/SF_6}$	Organics
$\boldsymbol{BCl_3, SF_6}$	Aluminum

Table 2.2 Etching gases for different material in Dry etching process.

Surface micromachining is another commercially important process that is widely used for fabrication of MEMS devices. In this approach, oxidized silicon coated with silicon nitride is used as a substrate. This is to make electrical isolation and also provide an anchor to hold the attached element. Silicon dioxide is used as the sacrificial layer and poly-silicon is selected as the structural material [1]. The surface micromachining material system is illustrated in table 2.3 which includes the types of material commonly used for structural, sacrificial, release etch and isolation layer [18, 19, 20].

Structural	Sacrificial	Release Etch	Isolation
Polysilicon	SiO_2	Buffered HF	$Si_3N_4 + SiO_2$
Polyimide	Aluminum	PAN etch	SiO_2
LPCVD $\mathbf{Si_3N_4 + Al}$	Poly-silicon	XeF_2	SiO_2
Aluminum	Photo-resist	Oxygen Plasma	SiO_2

Table 2.3 Material commonly used in surface micromachining technique.

Figure 2.4[7] demonstrates the surface micromachining method from starting point which is placing the pattern contact on the oxidized silicon and then depositing the sacrificial layer. Pattern structural layer is deposited on top of the sacrificial layer and at the final stage the pattern contact is removed to have the structural layer suspended.

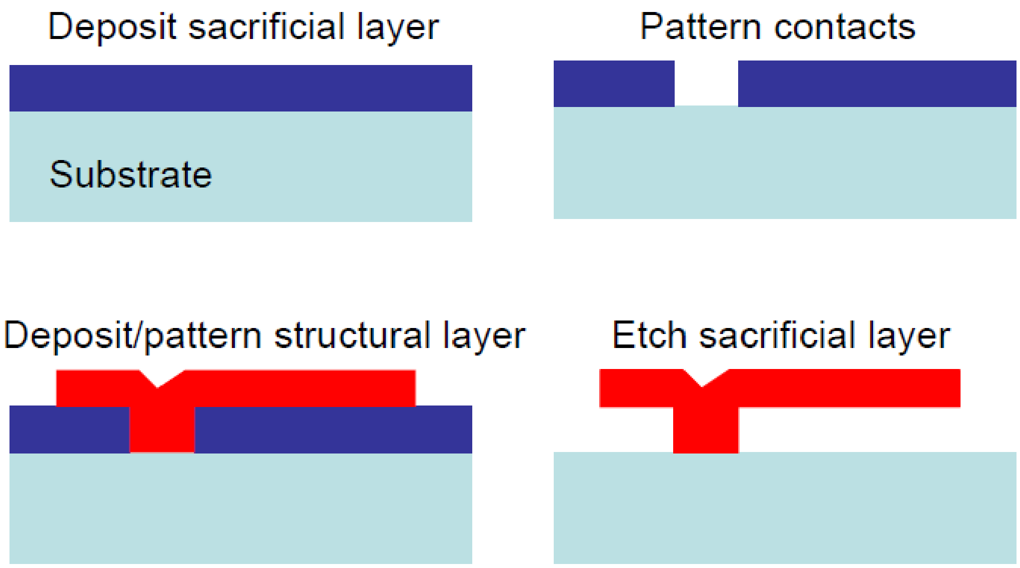

Figure 2.4 Surface micromachining [7].

Micromachining is compatible with standard CMOS fabrication which provides a critical enabling technology that allows mechanical components to be fabricated on a silicon substrate [1].

2.2 Cost of a typical MEMS devices

Figure 2.5 [7] illustrates the cost distribution of typical MEMS devices based on each production sector individually.

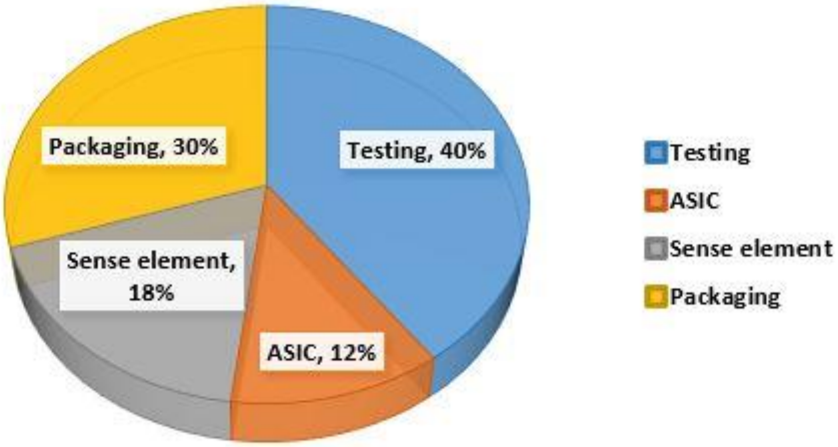

Figure 2.5 Cost distribution of a typical MEMS device [7].

It can be seen that the major portion of the total cost belongs to the testing phase which amounts to almost 40% of the overall unit cost. This shows how crucial and significant the testing sector is in the industry. Hence, MEMS testing is extremely important from economical point of view. Although, each manufacturer has its approach towards testing, MEMS devices are normally tested at two different stages. MEMS manufacturing tests is first performed at the wafer level and then at the packaging stage. Manufacturers also randomly select samples and perform sampling check on every fabrication run. Developing a test solution for MEMS devices to minimize the test time and reduce the costs is still a challenging research topic.

2.3 Microsystems general test approach in the industry

Automatic test equipment (ATE) is widely used in the industry to test devices after fabrication. To conduct manufacturing test hardware and software are developed by test engineers to carry out the testing task using ATE systems. The software directs the ATE to apply various electrical stimuli such as sine waves, triangle waves, pulses and digital signals to the device under test (DUT). The ATE [19] tester then observes the responses of DUT in order to determine whether the DUT is fault-free or not. The block diagram of general approach for device testing is shown in Fig 2.6.

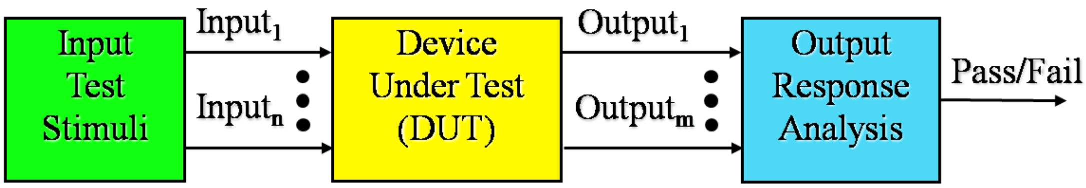

Figure 2.6 General micro-systems test approach

2.4 MEMS test solutions proposed in the literature

Developing test solutions for MEMS devices is proven to be a challenging task. This is mainly due to the multidisciplinary nature of MEMS systems where the input stimulus or the output response may not be electrical signals. In general, testing MEMS devices can be costly and may require sophisticated equipment to characterize performance parameters in different energy domains. There is a need for dedicated test solutions for MEMS devices to detect possible structural defects that can lead to the device failure. A fast and accurate on-chip method to determine the impulse response (IR) of MEMS devices is presented in [22]. This technique is able to provide a vast dynamic range in noisy environments with low power test signal. In [23], a contact free capacitive MEMS approach is proposed which is able to examine the surface potentials of a solid surface to generate a potential map. The information provided by the potential map is then used to defect analysis for MEMS devices. In [24], a tester architecture that supports calibration and testing of MEMS devices is implemented. This tester can manage the testing process through a specific hardware module that can reduce the test time. An electrical-only test procedure for MEMS accelerometer as an alternative to functional test is introduced in [25]. It presents a low cost MEMS test setup at the wafer level to detect parametric faults through screening MEMS devices prior to packaging. In [26], the micro-mechanical portion of MEMS structures is demonstrated as a black box that can be used as a good approximation for mechanical behavior to conduct manufacturing test. A base exciter is developed in [27] to trigger a MEMS device. This dynamic test solution is applicable at the wafer level. In [28], a solution is presented to test parallel MEMS sensors using an analog parallel test technique. This method can reduce the test time significantly for

MEMS batch process manufacturing. A Built-In-Self-Test (BIST) technique that can be applied to symmetrical micro structures is described in [29]. Self-test outputs have been used to detect the presence of asymmetry due to the defects. This approach can detect the structural defects due to manufacturing process. A MEMS test structure and measurement procedure is presented in [30] to extract the lateral conductivity of thin film such as aluminum and p-doped poly silicon. In [31], a set of electrostatically actuated MEMS test structures is presented to monitor MEMS fabrication process and measure material properties. A fully electrical test procedure for characterization of MEMS at the wafer-level is presented in [32]. In this approach a test setup to measure electrical and mechanical parameters of capacitive MEMS sensors has been developed. This test setup presents a fast wafer-level test solution for MEMS devices. A BIST solution for capacitive MEMS devices which is called dual-mode BIST technique is proposed in [33]. The control circuit in this technique only consists of several multiplexers and as a result the area overhead due to the test circuits is small. In [34], a technique to diagnose mechanical parameters of a cantilever-beam using electrical test stimulus is described. In this method, the MEMS response is mapped to the mechanical properties of the beam using a regression-based mapping technique. It is reported that this test solution can estimate the beam mechanical parameters with accuracy of 5% of the nominal values. A major class of MEMS sensors operate based on the principle of capacitance sensing where the MEMS sensor can be modeled by a variable capacitor. The parameters of interest in these sensors are detected through capacitance variations. Various test methods for this class of capacitive MEMS have been proposed in the literature [35, 36, 37, 38, 39, 40]. Most of the test methods in the literature rely on the test response evaluation in the time domain. In this work a new solution is presented in which the output response analysis is performed in the frequency domain. It is shown that a small variation of MEMS performance parameters translates into a measurable quantity in the frequency domain.

The rest of this thesis paper is organized as follows. The proposed test solutions are presented in chapter three and four respectively that are paper-based already published in relevant IEEE conferences. The test setup used to implement a resonant-based test method shows the variation of capacitance and resonance frequency within a fault free and faulty capacitive MEMS structure. The circuit model representing the idea with fabrication results according to the mathematical model and simulations are included in chapter five and the conclusions and results are summarized in chapter six.

Chapter3

Resonant-Based Test Method for MEMS Devices

Developing test solutions for MEMS devices is proven to be a challenging task. This is mainly due to the multidisciplinary nature of MEMS systems where the input stimulus or the output response may not be electrical signals. In general, testing MEMS devices can be costly and may require sophisticated equipment to characterize performance parameters in different energy domains. There is a need for robust test solutions for MEMS devices to detect possible structural defects that can lead to the device failure. A major class of MEMS sensors operate based on the principle of capacitance sensing.

PRINCIPLE OF OPERATION

A capacitive MEMS sensor is a variable capacitor where the variations of the capacitance from its nominal value are used to measure the inputs. Physical defects such as missing or shorted fingers, rigid or deformed arms affect either the nominal capacitance value or its variations with the bias voltage. Accurate measurement of a MEMS capacitance can reveal most of the structural defects. For a typical MEMS sensor, the capacitance variations are in the femto-farad range. To detect such small changes in the time domain, high resolution and accurate measurement circuits are required. These requirements are relaxed if the measurement is performed in the frequency domain. The schematic diagram of the proposed solution to conduct the measurement in the frequency domain is shown in figure.3.1. It includes a signal source of variable frequency to apply input signals and a response evaluator to observe the output signals. To conduct the test, a signal is applied to the circuit to determine the resonance frequency. At this frequency the voltage across the output which is composed of a series LC circuit drops sharply. To show how small variations of MEMS capacitance can be identified in the frequency domain, the changes of the resonance frequency with respect to the MEMS capacitance has been determined. The resonance frequency (f_{res}) of the circuit is obtained from $f_{res} = \frac{1}{2\pi\sqrt{LC}}$. The variations of the resonant frequency with respect to the

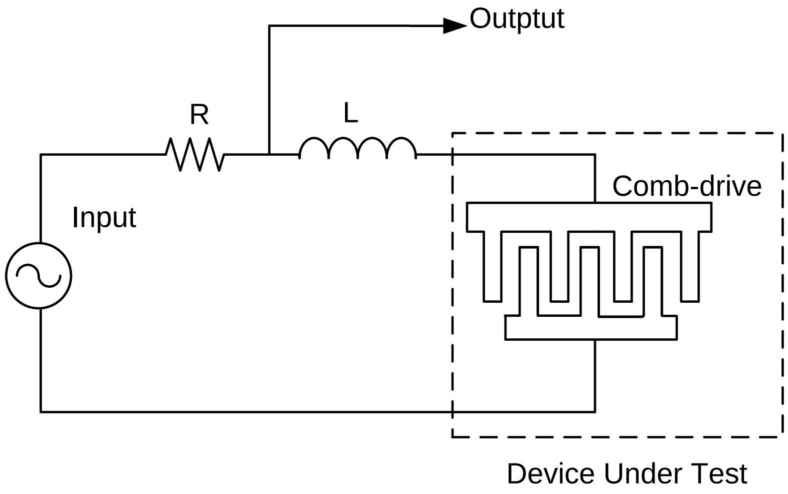

Fig. 3.1. Block diagram of the test solution for capacitive MEMS devices.

MEMS capacitance can be calculated form:

$$\frac{\partial f_{res}}{\partial C} = \frac{-1}{4\pi C\sqrt{LC}} = \frac{-f_{res}}{2C} \tag{1}$$

For a small capacitance variation we can write:

$$\nabla f_{res} \approx \frac{-1}{4\pi C\sqrt{LC}}\Delta C \approx \frac{-f_{res}}{2C}\Delta C \tag{2}$$

From (2) it can be seen that the variations of the MEMS capacitance, ΔC , is multiplied by a factor of $-f_{res}/2C$ which can be a significant number. For a case where $f_{res} =$

$1\ GHz$ and $C = 100\ fF$ the resonance frequency changes by 5KHz due to 10 atto-farad capacitance variations. Such a frequency shift can be measured in the frequency domain but measurement of 10 atto-farad variation in the time domain is a major challenge.

The schematic diagram of a MEMS comb-drive is shown in figure 3.2. It includes fixed and movable arms. The distance between the movable and fixed arms, x, in this structure changes due to the applied inputs. The variations of the capacitance with the distance between the arms can be determined from $C(x) = \varepsilon A/(d_o + x)$. Assuming $x << d_o$ from Taylor series $C(x)$ can be estimated by:

$$C(x) = C(1 + \frac{x}{d_0})^{-1} \approx C(1 - \frac{x}{d_0}) \tag{3}$$

where $C = \varepsilon A / d_0$. The resonance frequency variation as a function of movable arm displacement is obtained from:

$$\Delta f_{res} = \frac{1}{2\pi\sqrt{LC}} - \frac{1}{2\pi\sqrt{LC(x)}} \tag{4}$$

Substituting for $C(x)$ from (3) we have:

$$\Delta f_{res} = f_{res}\left[1 - (1 - \frac{x}{d_0})^{-1/2}\right] \tag{5}$$

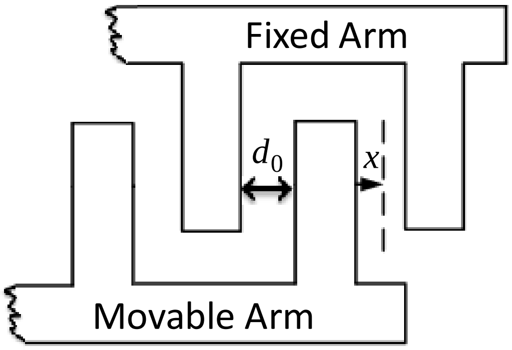

Fig.3.2. Schematic diagram of a linear comb drive used to determine variations of the resonance frequency with the displacements of the movable arm.

Using Taylor series estimation of:

$$(1-\frac{x}{d_0})^{-1/2} \approx 1+\frac{x}{2d_0} \qquad (6)$$

Equation (5) is simplified to:

$$\Delta f_{res} \approx f_{res}\left(-\frac{1}{2}\frac{x}{d_o}\right) \qquad (7)$$

As expected equation (7) indicates that a small displacement of the movable arm is multiplied by a significant factor of $-f_{res}/2d_o$ affecting the resonance frequency. This is consistent with the results obtained from equation (2).

To reduce the required test resources and the test time, instead of frequency the amplitude of the output can also be observed at the resonant frequency. In this case, the test signal can be applied at the frequency where the inductor resonates with the comb drive's nominal capacitance. The structural defects of the MEMS device are detected through observation of the output amplitude variations rather than the resonant frequency variations. The quality factor of the inductor in Fig.3.1 does not affect the performance of the circuit considerably if resonant frequency variations are observed. However, the quality factor of the inductor has a significant effect if the amplitude variations at the resonant frequency are observed.

An actual inductor has a small series resistance. The inductor L in figure 3.1 can be modeled by an ideal inductor, L_s, in series with a resistor, R_s. The magnitude of the impedance of L in series with the comb drive's capacitance is given by:

$$\left|Z(\omega)\right| = R_s\left[\sqrt{1+Q^2\left(\frac{\omega}{\omega_0}-\frac{\omega_0}{\omega}\right)}\right] \tag{8}$$

Where ω is the angular frequency, $\omega_0 = 1/\sqrt{L_s C}$ and Q is the quality factor at the resonant frequency which is determined from $Q = L_s\omega / R_s$. The variations of $\left|Z(\omega)\right|$ with frequency is plotted in figure 3.3. It can be seen that the value of the quality factor affects the impedance considerably.

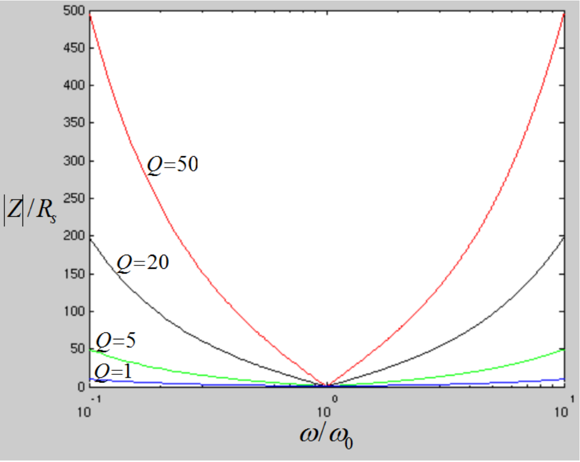

Fig.3.3. Effect of quality factor of the inductor on the variations of impedance.

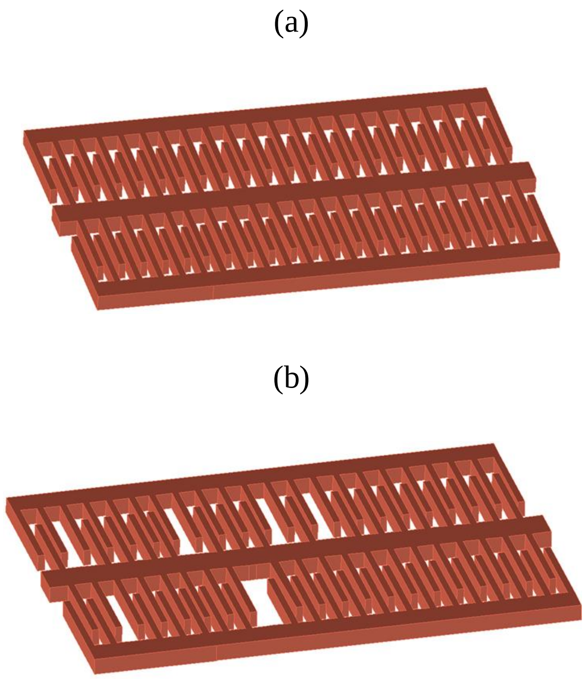

Fig. 3.4. (a) Implemented comb-drive used to evaluate the proposed test method. (b) Comb-drive with missing fingers used for fault analysis.

For the case where $\Delta\omega = \omega - \omega_0 << \omega_0$ the impedance can be simplified to:

$$|Z(\omega)| = R_s\left[\sqrt{1+\left(2Q\frac{\Delta\omega}{\omega_0}\right)^2}\right] \tag{9}$$

Assuming $2Q\Delta\omega/\omega_0 << 1$ and using Taylor series we have:

$$|Z(\omega)| \approx R_s\left[1-\frac{1}{2}\left(2Q\frac{\Delta\omega}{\omega_0}\right)^2\right] \tag{10}$$

The impedance variation $\Delta|Z(\omega)| = |Z(\omega)| - |Z(\omega_0)|$ can be calculated from

$$\Delta|Z(\omega)| \approx -2R_s\left(Q\frac{\Delta\omega}{\omega_0}\right)^2 = -2L_s\omega Q\left(\frac{\Delta\omega}{\omega_0}\right)^2 \tag{11}$$

Equation (11) indicates that the impedance variations and consequently the variations of the amplitude at the output in figure 3.1 is directly proportional to the quality factor of the employed inductor. Therefore to detect small variations of comb drive capacitance, a high Q inductor has to be employed.

SIMULATION RESULTS

To test the validity of the presented method, a MEMS comb drive was designed and simulated using Coventorware CAD tool. The circuit simulations were performed using Agilent's Advanced Design System (ADS). The implemented comb-drive in figure3.4 (a) was used to perform circuit level simulations. Fig 3.4(b) shows the same comb-drive with missing fingers which is used to observe the variations of the resonance frequency due to the physical defects.

Figure 3.5 presents the MEMS structure in Coventorware environment before and after applying the stimulus. It can be seen that the stimulated movable arm deflect by as much as 10nm. This displacement affects the MEMS nominal capacitance and consequently the resonant frequency in the test mode.

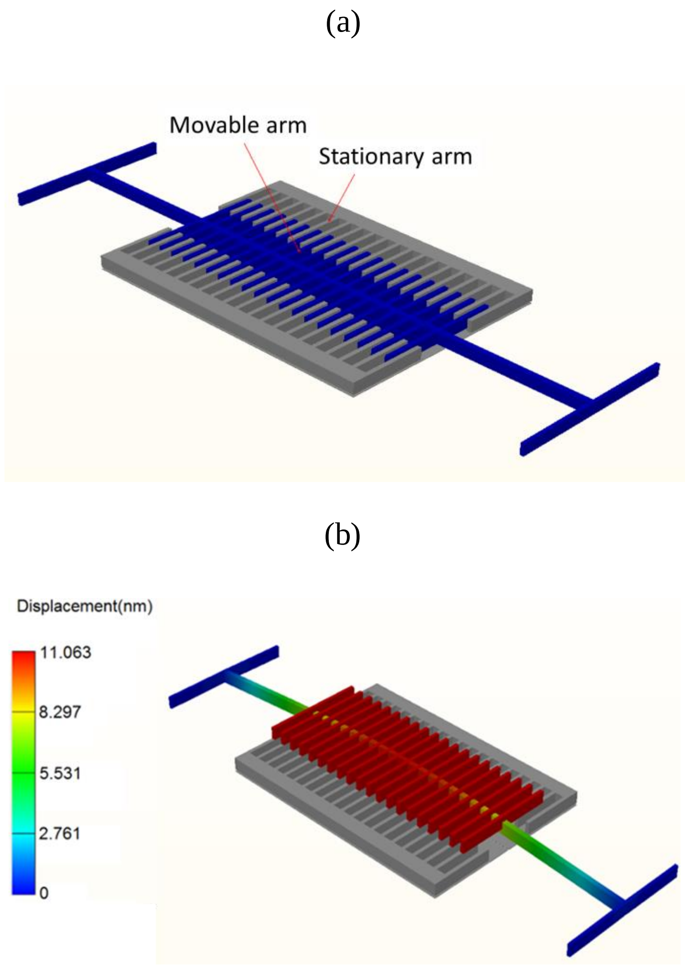

Fig.3.5. Implemented capacitive MEMS (a) before applying the stimuli and (b) after applying the stimulus.

The nominal capacitance of the structure as shown in Fig.3.6 remains close to 0.96 pf up to 3.0 GHz.

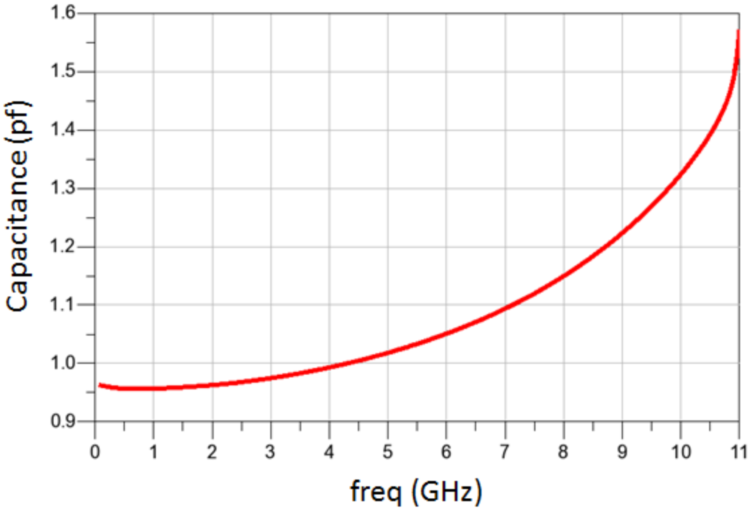

Fig.3.6. Plot of the capacitance with respect to frequency sweep.

At higher frequencies the capacitance increases due to the high frequency effects of the substrate used to implement the comb drive. The test circuit is designed to ensure that the resonance frequency falls below 3.0 GHz to avoid the undesired effects on the test results at higher frequencies.

The test setup in figure 3.1 with L_s=23nH, R_s=2Ω and R=50Ω was simulated using ADS. The output signal is shown in Fig.3.7. It can be seen that the signal falls sharply at the resonance frequency of 2.81 GHz. The effects of missing fingers on the MEMS capacitance and resonance frequency have been summarized in Table I. The variations of the resonance frequency is linear and as the number missing fingers increases as expected the capacitance decreases and the resonance frequency increases.

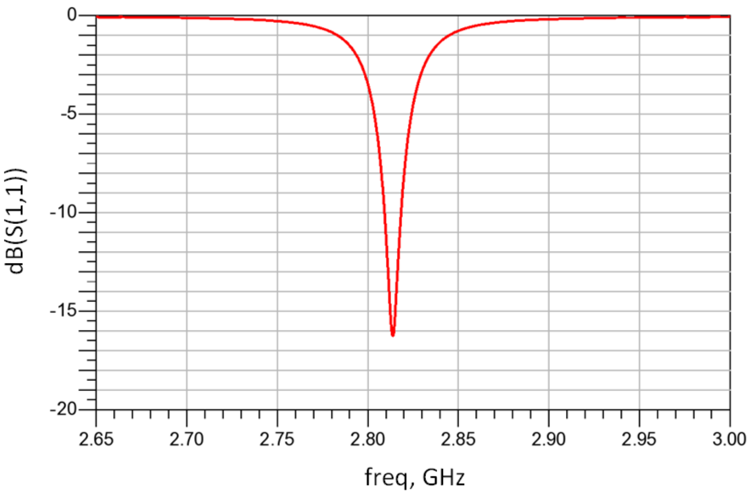

Fig.3.7. Insertion loss of the circuit indicating that the inserted inductance and the MEMS capacitance resonate at 2.81GHz.

TABLE II.VARIATIONS OF PERFORMANCE PARAMETERS OF THE IMPLEMENTED COMB DRIVEF WITH SHORT FINGERS AND TILTED MOVABLE ARM.

	Output at the resonant frequency(dB)	f_{res} (GHz)	Δf_{res} (MHz)
Short fingers	-12.031	2.8179	5
Tilted movable arm by 3 degrees	-24.404	2.8234	9

The variation of output with respect to the frequency sweep for short fingers and tilted movable arm is shown in Table II. Simulations were also performed to see the effect of a high Q inductor on the output amplitude variations. The results indicate that the amplitude of the output signal varies approximately 1.0 dB from the reference value for each missing finger when an inductor with $Q = 30$is used.

TABLE I.VARIATIONS OF PERFORMANCE PARAMETERS OF THE IMPLEMENTED COMB DRIVEF WITH MISSING FINGERS.

Number of missing fingers	Total Capacitance (pF)	ΔC (fF)	f_{res} (GHz)	Δf_{res} (MHz)
0	0.934	0	2.8136	0
1	0.928	6	2.8141	0.5
2	0.921	13	2.8144	0.8
3	0.914	20	2.8149	1.3
4	0.907	27	2.8152	1.6
5	0.898	36	2.8158	2.2
6	0.892	42	2.8162	2.6
7	0.885	49	2.8167	3.1

Chapter 4

Test Method for Capacitive MEMS Devices Utilizing Pierce Oscillator

In this paper a test method for MEMS devices is presented in which physical defects are detected in the frequency domain rather than the time domain. A resonator that can be part of a read out circuits utilized to test capacitive Micro-Electro-Mechanical Systems (MEMS). The proposed technique is based on the principle of resonant frequency where variations of the resonant frequency are observed to detect structural defects. To verify the validity of the proposed approach, a MEMS comb-drive is designed and fabricated. Measurement and simulation results indicate that the proposed method can be used to capture common comb-drive defects such as missing or broken fingers, shorted fingers and tilted arms. In this work, Pierce oscillator is utilized to conduct test on MEMS devices. The proposed method has a good sensitivity and detects common faults of capacitive MEMS devices.

PRINCIPLE OF OPERATION

Fig.4.1 shows the block diagram of the proposed test setup. The circuit is implemented using 65nm CMOS technology. ARLC tank is utilized to ensure operation at the desired frequency and support a good stability against external disturbances. The circuit diagram includes three delay cells to form a delay line. The RLC tank acts as a selective tuner to affect the output response through the feedback resistor. At the resonant frequency, the input and the output of the delay line is shorted and the delay cells form a ring oscillator. As shown in Fig.4.1, the MEMS device is connected to the oscillator in series with a capacitor, C_1. This capacitor is used as a reference and its value is chosen to be equal to the nominal capacitance of the MEMS device.

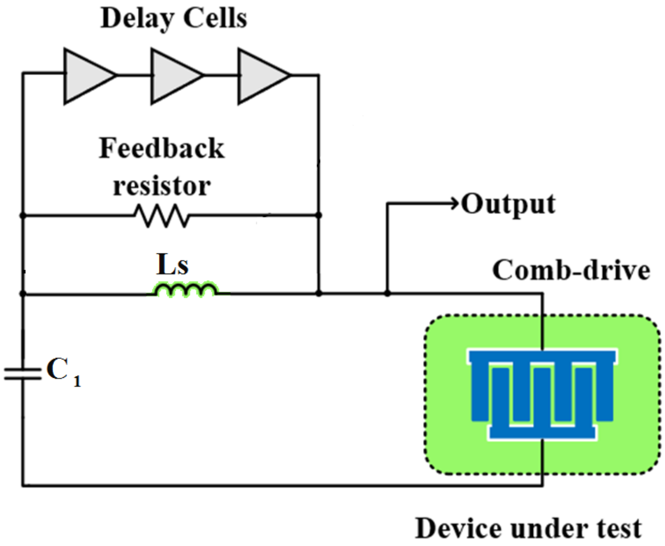

Fig.4.1 Block diagram of the proposed test solution.

Fig.4.2presents the schematic diagram of a differential delay cell used to implement the oscillator. The delay cell is optimized to minimize the jitter. The tail current which is commonly used for a differential pair is removed to increase the speed of transition from low to high level. The tail current in a differential pair contributes heavily to the common mode and power supply rejections. However, the tail current can be removed for a differential delay cell with digital level outputs to improve jitter performance. The tail current in a differential pair limits the maximum current. As a result the transition from a low level to a high level the parasitic capacitors are charged with a limited current which increases the time required to complete the transition. This will give a higher chance to the noise to corrupt the switching level and introduce jitter to the oscillator.

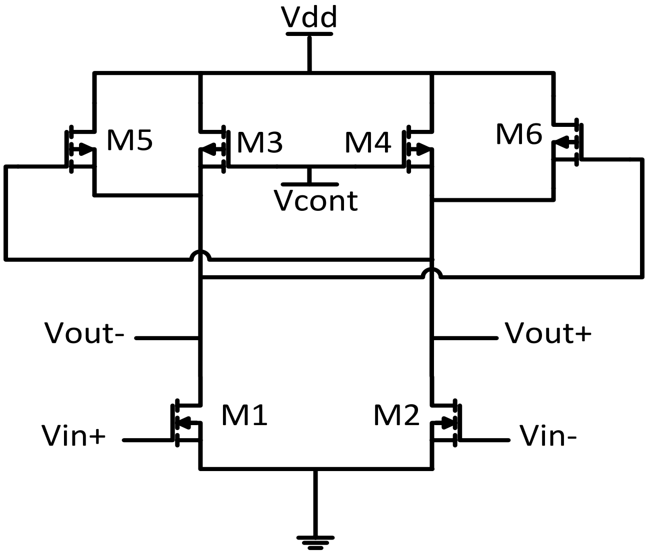

Fig.4.2. Schematic of the differential cell.

PMOS transistors in Fig.4.2, M3 and M4, act as variable resistor loads to control the delay over a certain range. M5 and M6 are added to further increase the speed of transitions from a low level to a high level. The aspect ratio of $\frac{W}{L} = \frac{3.2}{0.2}(\mu m)$is chosen for M1-M2 transistors and M3-M6 are sized to have$\frac{W}{L} = \frac{3.8}{0.2}(\mu m)$ to achieve the oscillation frequency of 1.1 GHz. The feedback network stabilizes the frequency and keeps the oscillator in the linear region of operation, even though in practice obtaining a pure linear oscillator is not feasible [41]. A feedback resistor is also inserted to change the input impedance of the oscillator and maintain proper matching so that the resonator can drive the delay cells.

The resonance frequency (f_{res}) of the circuit can be obtained from $f_{res} = \frac{1}{2\pi\sqrt{L_s C}}$ where $C = (C_1 C_{MEMS}) / \ (C_1 + C_{MEMS})$.

The variations of the resonance frequency of the implemented test circuit with MEMS capacitance changes can be written as:

$$\frac{\partial f_{res}}{\partial C} = \frac{-1}{4\pi C\sqrt{L_s C}} = \frac{-f_{res}}{2C} \qquad (1)$$

Since the capacitance variation is very small, it can be presented as:

$$\Delta f_{res} \approx \frac{-1}{4\pi C\sqrt{L_s C}}\Delta C \approx \frac{-f_{res}}{2C}\Delta C \qquad (2)$$

It can be seen that the capacitance variation (ΔC) is multiplied by a factor of $-f_{res}/2C$ which is a significant value.The above analysis indicate that the detection of MEMS defects in the frequency domain is much easier than the time domain. For instance, a defect causing 10fF variation from a nominal value of 1pF in the time domain can alter the resonant frequency of 1.0GHz by more than 10MHz. Such a significant variations of frequency can readily be measured in the frequency domain while measurement of 10fF in the time domain is a challenging task.

SIMULATION AND MESUERMENT RESULTS

To verify the validity of the proposed method, simulations were carried out using advanced design system (ADS) simulation tool from Agilent with TSMC 65nm CMOS technology. In addition, a MEMS comb-drive was designed and fabricated to validate the proposed test solution.Fig.4.3 (a) shows the implemented MEMS comb-drive structure in Coventorware environment in the steady state without a test stimulus and Fig.4.3 (b) presents the response after excitation with a test stimulus. It can be observed that the MEMS movable arm is displaced by about 10nm in response to the applied input.

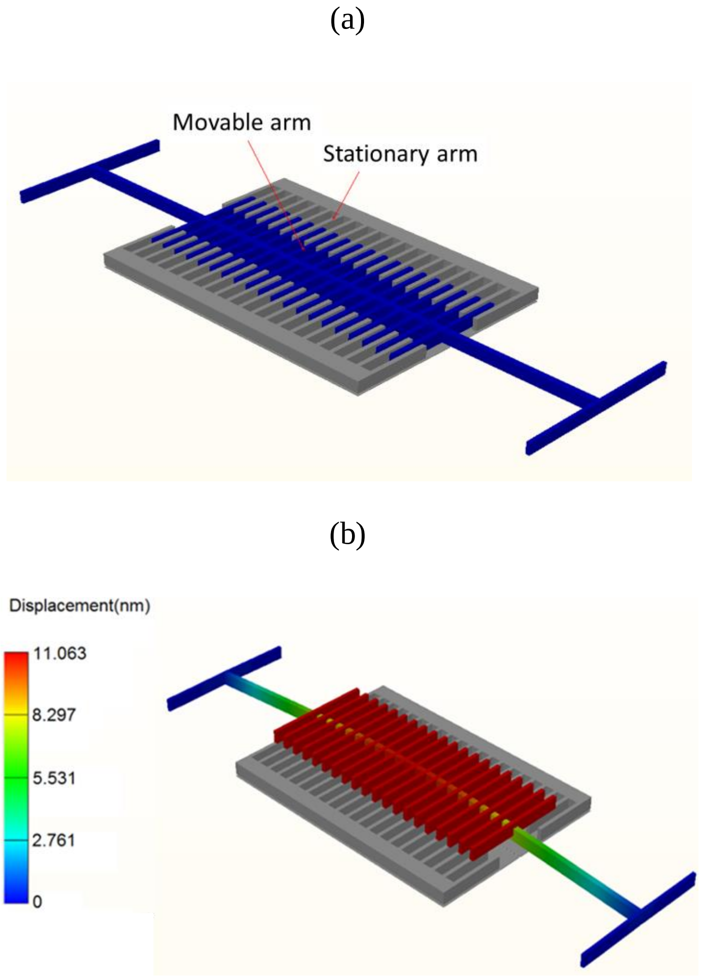

Fig.4.3. Implemented MEMS comb-drive (a) steady state without a test stimulus and (b) excited with a test stimulus.

This displacement affects the capacitance of the comb-drive by about five femto-Farads. Such a minor capacitance variation is extremely difficult to measure in the time domain. However, in the frequency domain the 5fF variation translates to a significant change in the frequency of the implemented oscillator. The response of the oscillator for a fault-free comb-drive is shown in Fig.4.4.

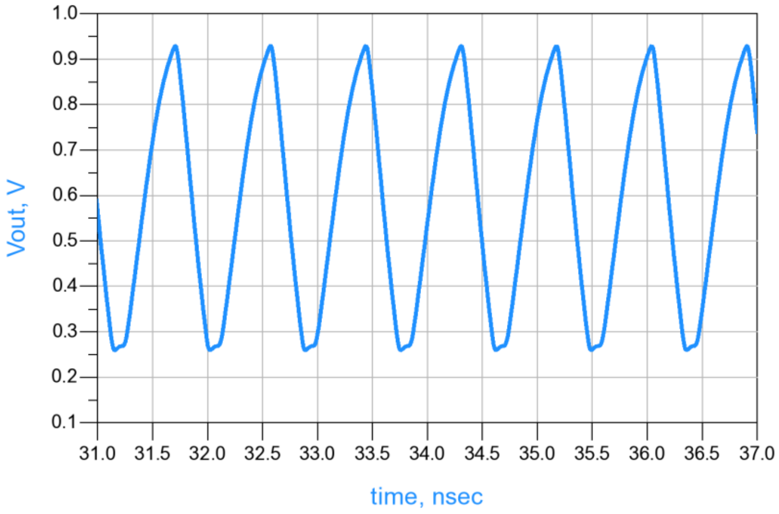

Fig.4.4 Output of the oscillator running at 1.07GHz.

It can be seen that the periodic sinusoidal signal is generated with a constant envelope. The voltage swing of 690 mV was obtained which is the normal operating mode. From Fig.4.4, the measured time period of the output signal is about 0.93ns which represent the oscillation frequency of 1.07 GHz.

For the purpose of fault analysis, different faults were injected to observe the effect of the output. In addition to the frequency variations, the deviations of the amplitude can also be observed to detect possible defects. Fig.4.5 presents the effects of missing fingers on the output frequency response. It can be seen, as the number of missing fingers increases the output voltage swing grows and the frequency of oscillation changes.

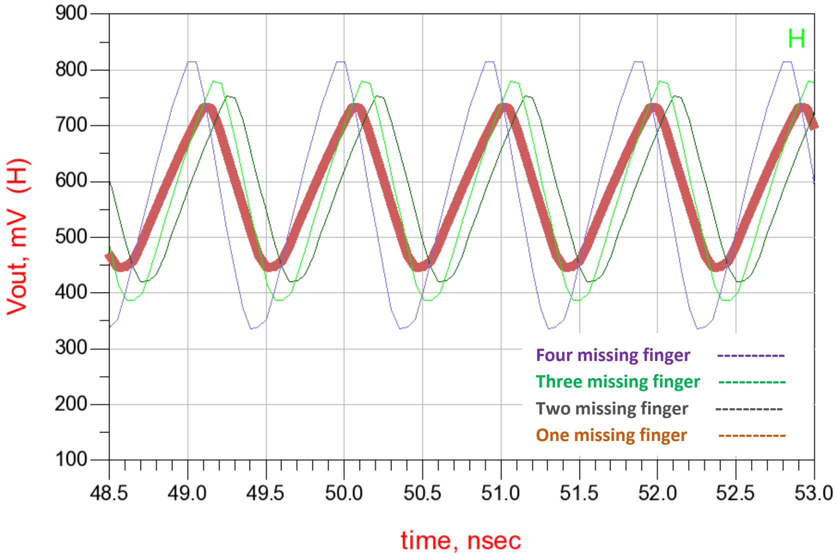

Fig.4.5. Output response according to the comb-drive missing fingers.

Based on the simulation results each missing finger corresponds to approximately five femto-Farads reduction in the total capacitance which will corresponds to almost 5MHz resonance frequency shift. Simulation results for different cases of missing fingers are summarized in Table. I. The variation of frequency with missing fingers is linear and for each missing finger the oscillation frequency rises by about 4.6MHz. The table also presents the amplitude variations with missing comb-drive fingers. It can be seen that the amplitude variation with frequency is not linear.

TABLE I.VARIATIONS OF PERFORMANCE PARAMETERS ACCORDING TO MISSING FINGERS OF THE IMPLEMENTED MESMS STRUCTURE.

Number of missing fingers	Total capacitance (fF)	ΔC (fF)	Period (ns)	f_{res} (GHz)	Δf_{res} (MHz)	Voltage swing (mV)
0	52	0	0.931	1.0741	0	302
1	47.2	4.8	0.927	1.0787	4.6	324
2	42.3	9.7	0.924	1.0822	8.1	349
3	37.2	14.5	0.920	1.0869	12.8	386
4	32.4	19.6	**0.**918	1.0893	15.2	421
5	27.5	24.5	0.915	1.0928	18.7	476
6	23.3	28.7	0.911	1.0976	23.5	514

A comb-drive was fabricated and tested as a proof of concept. Fig.4.6 (a) shows photos of the fabricated comb-drive using a gold-based surface micromachining process. The measured return loss of the comb-drive using Agilent's E5016B network analyzer is shown in Fig.4.6 (b). To evaluate the fault coverage of the proposed test solution, physical faults were injected into samples of the fabricated comb-drive.

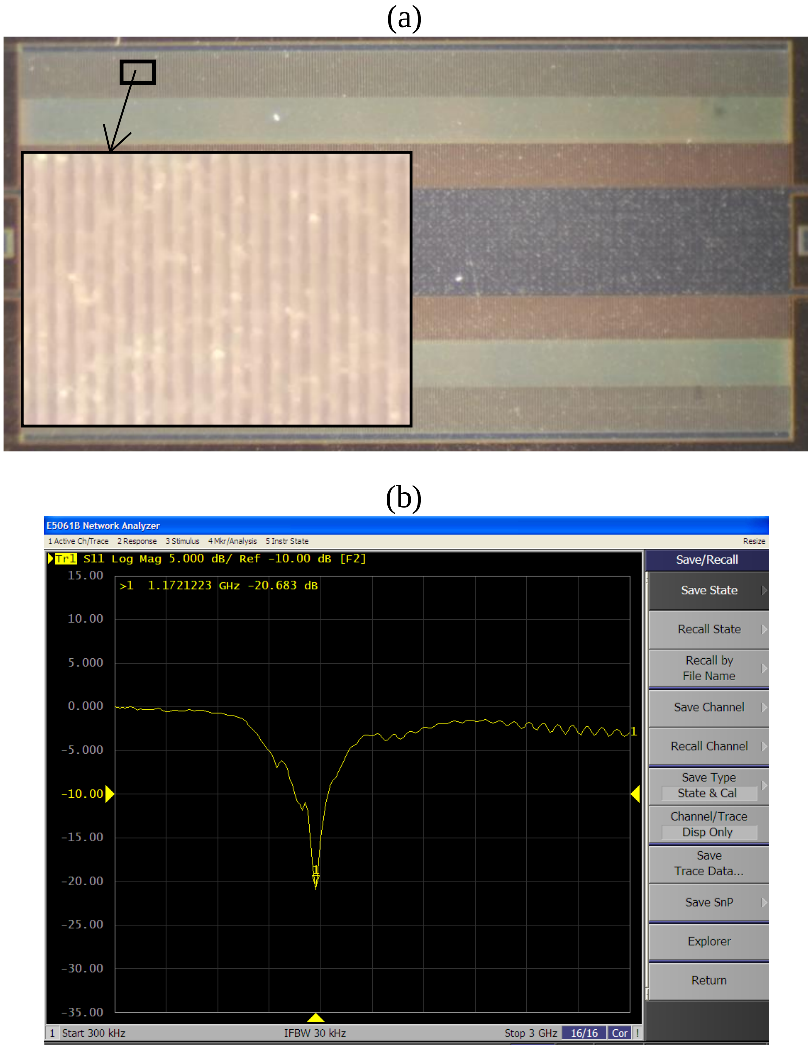

Fig.4.6. (a) Photos of the fabricated comb-drive using a gold-based surface micromachining process, (b) Measured return loss of the fault-free comb-drive.

The measured S-parameters for both faulty and fault-free comb-drives are shown in Fig.4.7. It can be seen that the structural defects affect the S-parameters considerably. The measured S-parameters were used to extract circuit models for both faulty and fault-free comb-drives. Then the circuit models were imported to the ADS environment for fault analysis.

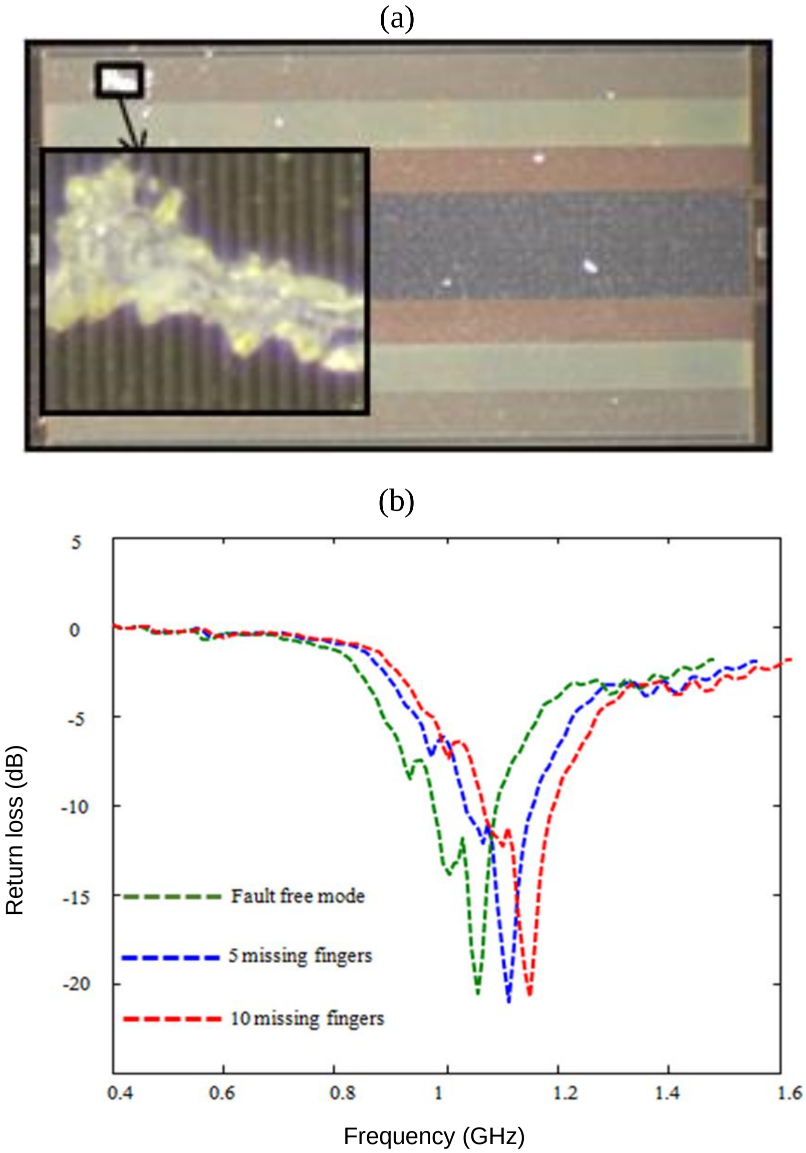

Fig.4.7 (a) Photo of a faulty comb-drive (b) Return loss for both faulty and fault-free comb-drives.

The results indicate that the proposed test solution can successfully detect missing, broken and shorted fingers. The resonant frequency in this case changes by about 5.5 MHz for each missing finger which is close to the results obtained through simulations.

Chapter 5

Self-Resonation Test Methodology for Capacitive MEMS devices

Developing test solutions for MEMS devices is proven to be a challenging task. This is mainly due to the multidisciplinary nature of MEMS systems where the input stimulus or the output response may not be electrical signals. In general, testing MEMS devices can be costly and may require sophisticated equipment to characterize performance parameters in different energy domains. A dedicated test solution for MEMS devices is needed to detect possible structural defects that can lead to the device failure. Test solutions for MEMS devices to evaluate their performance in different energy domain [42] are needed. In general, micro-system testing poses certain challenges due to the high density and complexity of fabricated components which limits the controllability and observability. Test for MEMS devices, in addition to the electrical test stimuli, may require signals in other domains such as mechanical, temperature or light inputs to characterize the device by stress, strain or heat transfer analysis [43]. Ultimately, a series of tests should be performed prior to device deployment in the field. In the area of semi-conductor testing, mixed-signal circuits and MEMS devices introduce greater challenges in comparison with digital circuits due to their component design complexity and larger sample space for testing purposes. A major class of MEMS sensors operate based on the principle of capacitance sensing where the MEMS device can be modeled by a variable capacitor. The parameters of interest in these sensors are detected through capacitance variations. As an example, in automotive industry MEMS accelerometer is widely used as an innovative approach to trigger vehicle airbag. Capacitive MEMS sensors are also used in many other applications such as vibration monitoring, shock detection, navigation systems, air blast pressure sensor. At the heart of accelerometers, a single or multiple comb-drives are used that are operating based on the capacitance sensing. Various test methods for capacitive MEMS have been proposed in the literature [35-40]. A Built-In-Self-Test (BIST) technique that can be applied to symmetrical structures is presented in [29]. Self-test techniques have been employed to detect the presence of asymmetry due to the defects. This approach can detect manufacturing related structural defects. A MEMS test structure and measurement procedure is presented in [30] to extract the lateral conductivity of thin film such as aluminum and p-doped poly silicon. In [31], a set of electrostatically actuated MEMS structures is presented to monitor MEMS fabrication process and measure material properties. A fully electrical test method for MEMS devices at the wafer-level is presented in [32]. In this approach a test setup to measure electrical and mechanical parameters of capacitive MEMS sensors has been developed. This test solution presents a fast wafer-level verification for MEMS devices. A BIST solution for capacitive MEMS devices which is called dual-mode BIST technique is presented in [33]. The control circuit in this technique only consists of several multiplexers, as a result the area overhead due to the test circuits is negligible. In [34], a technique to detect mechanical parameters of a cantilever-beam using electrical test stimulus is described. In this solution, the MEMS response is mapped to the mechanical properties of the beam using a regression-based mapping technique. It is reported that this test solution can estimate the beam mechanical parameters with accuracy of 5% of the nominal values. Intensive researches are conducted to materialize MEMS-CMOS integration [22-23]. There are many advantages in using MEMS devices such as low parasitic, small sizes and low costs [24]. Capacitive sensors can benefit from MEMS technology [25] which can reduce the costs and improves the performance [26].Most of the test methods for MEMS devices in the literature rely on the test response evaluation in the time domain. In this work a new solution is presented in which the output response analysis is performed in the frequency domain. It is shown that a small variation of MEMS performance parameters translates into a measurable quantity in the frequency domain.

PRINCIPLE OF OPERATION

A capacitive MEMS sensor is in fact a variable capacitor where the variations of the capacitance from its nominal value are used to measure the inputs. Comb-drive is a commonly used capacitive MEMS for many applications. Physical defects such as missing, broken or shorted fingers, rigid or deformed arms affect the nominal MEMS capacitance value or alter its variations with the bias voltage. Accurate measurement of a MEMS capacitance can reveal most of the structural defects. For a typical MEMS capacitive sensor, the capacitance variations are in the femto-farad range and in certain cases in the atto-range. To detect such small changes in the time domain, high resolution and accurate measurement circuits are required. These requirements are relaxed if the measurements are performed in the frequency domain. The schematic diagram of the proposed solution to conduct the measurement in the frequency domain is shown in Fig. 5.1. It includes a signal source of variable frequency with known internal impedance to apply input signals to a spiral inductor in series with a capacitive MEMS device to observe the output signals. To conduct the test, a signal is applied to the circuit to determine the resonance frequency. At this frequency the voltage across the output which is composed of a series LC circuit drops sharply. Due to the interaction between the capacitance and the inductance, the impedance of these components cancel out each other at the resonant frequency [20].

In order to validate the proposed test method, a comb-drive and a spiral inductor was designed. The reason for selecting spiral inductor is due to the fact that a spiral inductor can readily be fabricated using the available CMOS technologies and it presents a relatively good quality factor [21].

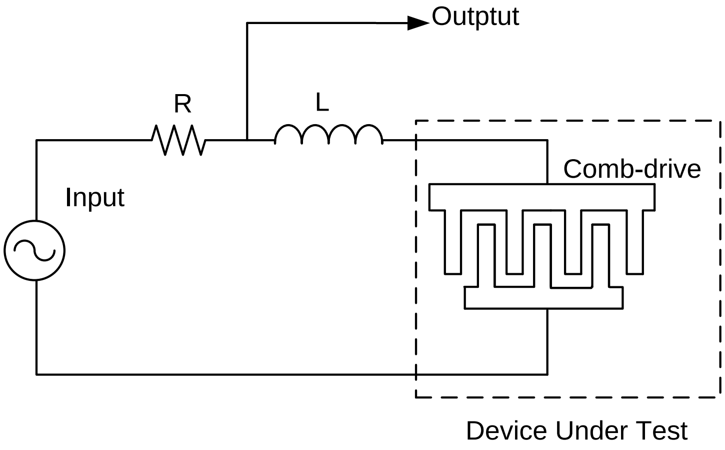

Fig. 5.1 Block diagram of the test solution for capacitive MEMS devices.

Based on the principle of operation for capacitive MEMS, the capacitor is stimulated by applying the electrical input signals. The stored energy on the capacitor affects the electrostatic force on the movable and stationary arms of the capacitive MEMS. A comb-drive is designed and simulated to model a capacitive MEMS device. The implemented comb-drive includes two stationary and one movable arms which are attached to a suspension beam from both sides. The MEMS comb-drive, without applying the stimuli, can be modeled as parallel plate spring-suspended capacitor that follows the basic electrostatic actuation rule that is displayed in figure 5.2.

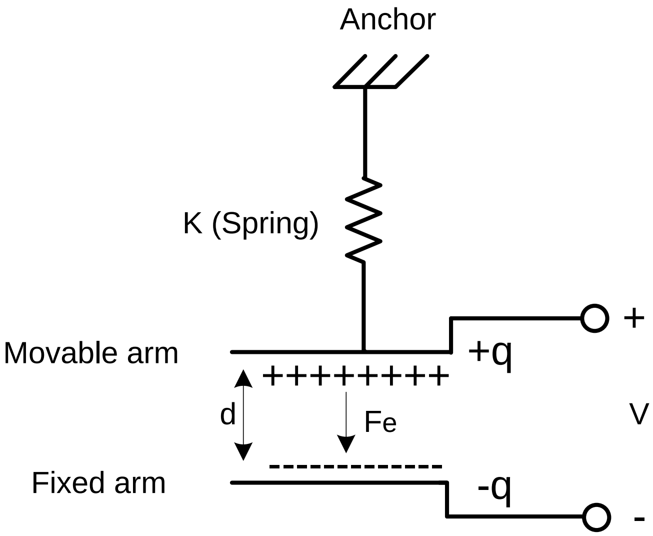

Fig.5.2. Fundamental diagram of the spring-suspended model of a parallel plate capacitor.

From the principle of operation for electrostatic actuators, we can write:

$$F_e = \frac{q^2}{2\varepsilon A} \qquad (1)$$

Where q is the total charge stored on the capacitor, A is the capacitor plate area and ε is the permittivity. Equation (1) represents the relationship between the stored energy in a capacitor and the electrostatic force (F_e) which is applied to the movable and stationary component. It can be observed that F_e is not a function of the distance between the plates. This potentially can ease the test procedure as the structural collapse of the capacitive MEMS can be avoided in the testing phase. On the other hand based on the Hooke's law $F_e = ky$ where k and y are the spring constant and displacement of the spring respectively. When MEMS capacitor experiences an applied voltage and consequently electrostatic force, the distance between the plates (d) changes from d_0 to $d_0 - y$ where d_0 is the free-standing distance. In the steady state, the electrostatic force cancels out the mechanical force in equation (1) and thus we can write:

$$d = d_0 - y = d_0 - \frac{F_e}{k} = d_0 - \frac{\frac{q^2}{2\varepsilon A}}{k} \qquad (2)$$

On the other hand, the overall voltage across the capacitor could be written as:

$$V = \frac{q}{C} = \frac{q}{\frac{\varepsilon A}{d}} = \frac{q(d_0 - \frac{\frac{q^2}{2\varepsilon A}}{k})}{\varepsilon A} \qquad (3)$$

$$V = q(\frac{d_0}{\varepsilon A} - \frac{q^2}{2\varepsilon^2 A^2 k}) \qquad (4)$$

The above equations show that as the stored charge (q) increases, the electrostatic force between the plates increases by q^2. In order to balance the electrostatic force at equilibrium, the suspension beam needs to be stretched from its rest position.

Mathematical Approach for Capacitance Variation

The main parameter that changes according to the capacitance variation is the resonance frequency. To show how small variations of MEMS capacitance can be identified in the frequency domain, the changes of the resonance frequency with respect to the MEMS capacitance has been determined. The resonance frequency (f_{res}) of the circuit is determined from $f_{res} = \frac{1}{2\pi\sqrt{LC}}$. Accordingly, the variations of the resonant frequency with respect to the MEMS capacitance can be calculated form:

$$\frac{\partial f_{res}}{\partial C} = \frac{-1}{4\pi C\sqrt{LC}} = \frac{-f_{res}}{2C} \tag{5}$$

For a small capacitance variation we can write:

$$\Delta f_{res} \approx \frac{-1}{4\pi C\sqrt{LC}}\Delta C \approx \frac{-f_{res}}{2C}\Delta C \tag{6}$$

From (6) it can be seen that the variations of the MEMS capacitance, ΔC, is multiplied by a factor of $-f_{res}/2C$ which can be a significant number. For a case where $f_{res} = 1\ GHz$ and $C = 100\ fF$ the resonance frequency changes by 5KHz due to just 10 atto-farad capacitance variations. Such a frequency shift can be readily measured in the frequency domain but measurement of 10 atto-farad variation in the time domain is a major challenge. The schematic diagram of the MEMS comb drive used to determine the variations of the resonance frequency is shown in Fig. 5.3.

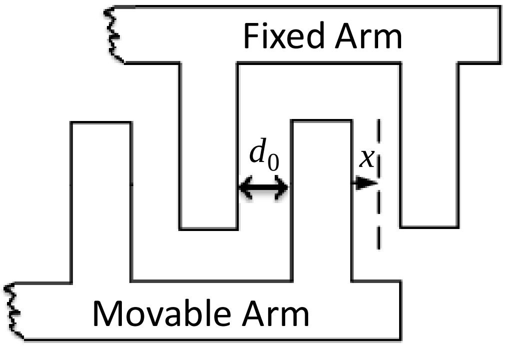

Fig. 5.3. Schematic diagram of a comb drive used to determine the variations of the resonance frequency with respect to the displacements of the movable arm.

It includes fixed and movable arms. The distance between the movable and fixed arms is marked by x whichvaries according to the applied inputs. The variations of the capacitance with the distance between the arms can be determined from $C(x) = \varepsilon A/(d_o + x)$. By expanding the Taylor series about $x = -d_0$ for $C(x)$ we can write:

$$C(x)=\sum_{n=0}^{\infty} \frac{C^n(d_0)}{n!}(x+d_0)^n \qquad (7)$$

$$\frac{\partial C(x)}{\partial x} = \frac{-\varepsilon A}{(d_0+x)^2} \qquad (8)$$

$$\frac{\partial^2 C(x)}{\partial x^2} = \frac{2\varepsilon A}{(d_0+x)^3} \qquad (9)$$

$$\frac{\partial^3 C(x)}{\partial x^{3n}} = \frac{-6\varepsilon A}{(d_0+x)^4} \qquad (10)$$

By taking the derivatives, the expression for $C(x)$becomes:

$$C(x)=C(d_0) + C'(d_0)(x+d_0) + \frac{C''(d_0)}{2!}(x+d_0)^2 + \cdots + \frac{C^n(d_0)}{n!}(x+d_0)^n \qquad (12)$$

Assuming $x << d_o$, the Taylor series of $C(x)$ can be estimated from:

$$C(x) = C(1+\frac{x}{d_0})^{-1} \approx C(1-\frac{x}{d_0}) \qquad (13)$$

where $C = \varepsilon A / d_0$. The resonance frequency variation as a function of movable arm displacement is obtained from:

$$\Delta f_{res} = \frac{1}{2\pi\sqrt{LC}} - \frac{1}{2\pi\sqrt{LC(x)}} \qquad (14)$$

Substituting for $C(x)$ from (13) we have:

$$\Delta f_{res} = f_{res}\left[1-(1-\frac{x}{d_0})^{-1/2}\right] \qquad (15)$$

Using Taylor series we have:

$$(1-\frac{x}{d_0})^{-1/2} \approx 1+\frac{x}{2d_0} \qquad (16)$$

Equation (15) is simplified to:

$$\Delta f_{res} \approx f_{res}\left(-\frac{1}{2}\frac{x}{d_o}\right) \qquad (17)$$

As expected equation (17) indicates that a small displacement of the movable arm is multiplied by a significant factor of $-f_{res}/2d_o$ affecting the resonance frequency. This is consistent with the results obtained from equation (6).

To reduce the required test resources and the test time, instead of frequency the amplitude of the output can also be observed at the resonant frequency. In this case, the test signal can be applied at the frequency where the inductor resonates with the comb drive's nominal capacitance. The structural defects of the MEMS device are detected through observation of the output amplitude variations rather than the resonant frequency variations. However, the quality factor of the inductor has a significant effect if the amplitude variations at the resonant frequency are observed. To select an inductor for the purpose of testing MEMS devices, special attention needs to be given to the performance parameters of the inductor with respect to the area overhead and also the desired frequency of operation.

In general, practical inductors that are implemented on-chip are in the range of 20 nano-Henry or lower [21]. Aside from the large area overhead of spiral inductors, there is an important problem that involves a considerable loss due to the skin effect that can lead to current distortion [21]. Thus, relative optimization with several trade-offs is required to implement the spiral inductor. There are different geometrical layouts for inductor implementation. The hexagonal format is preferred over square, octagonal or circular shapes. Figure 5.4(a) represents the parameters of the hexagonal spiral inductor that need to be taken into consideration. In this figure W is the metal width, S represents the edge to edge spacing between the adjacent turns, d_{in} and d_{out} are the inner and the outer diameters respectively. The number of turns is a key design factor in spiral inductor design [22].The hexagonal inductor was implemented using Advance Design System CAD tool from Agilent as shown in figure 5.4 (b).

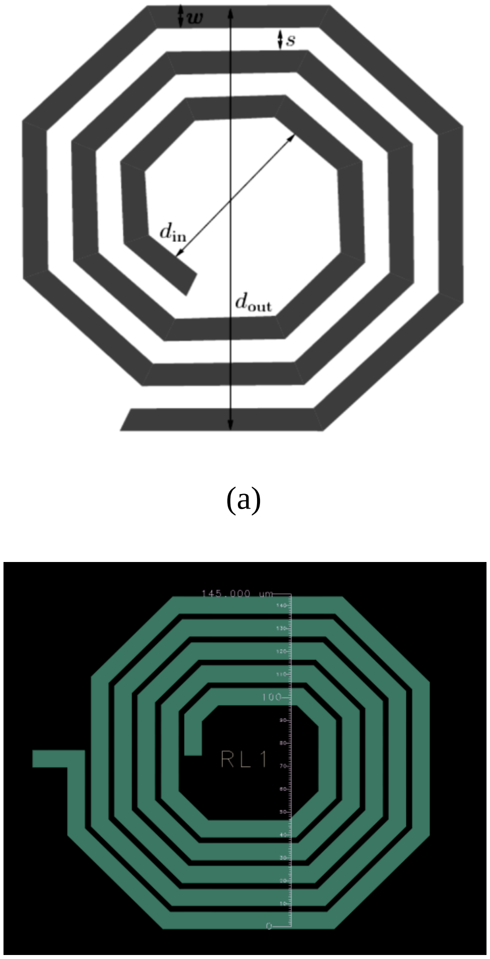

(a)

(b)

Fig. 5.4 Hexagonal inductor parameters (a) Hexagonal schematic (b) Layout of the implemented inductor in ADS.

The following constraints on the design space are imposed. The fill ratio, ρ, is chosen to be $0.1 < \rho < 0.9$ where$\rho = \frac{d_{out}-d_{in}}{d_{out}+d_{in}}$[22]. Another significant design parameter is S/W ratio which normally is selected to be at less than “1”for the available fabrication technologies for on-chip inductors. Below is an empirical formula that can represent the inductance of a spiral inductor [23]:

$$L_{hex} = 2.41 \times 10^{-3} n^{5/3} d_{avg} \log(4/\rho) \qquad (15)$$

d_{avg} is the average diameter which is $\frac{d_{in}+d_{out}}{2}$.

The starting point for the spiral inductor design was the required frequency of operation. Since in this work the gigahertz range is targeted then the capacitance of the Pico-Farad range and the inductance of nano-Henry range are desired. The frequency range was limited to less than five gigahertz for the purpose of certain application and the total capacitance obtained from the comb-drive was in the range of 100 femto-Farad to 1 pico-Farad. From the capacitance value and the upper limit for the resonant frequency equation, $\frac{1}{2\pi\sqrt{LC}} < 5GHz$, the inductance is required to be in the range of 2 to 10 nano-Henry.

It is necessary to properly model the desired on-chip inductor. There are couple of methods available in the literature to perform this task. Segment circuit model [22]is a simple approach by using a separate lumped π models for every single segment of desired shape. In hexagonal case with 6 turns we would have had $8\times 6 = 48$ separate lumped π model. Furthermore some additional parameters are also needed to model the coupling among the segments which adds to the complexity of the design. There is considerable research in the literature [24, 25, 26, 27] to model spiral inductors based on the lumped circuit model. The desired hexagonal inductor is represented by its equivalent π model. Figure 5.6 exhibits the π circuit model of the inductor. L and R_s are the series inductance and resistance respectively. C_s is the feed-forward capacitance. In fact, the implementation of the hexagonal inductor was carried out on silicon substrate; hence we had to consider the substrate capacitance, C_{si} , substrate-oxide capacitance, C_{ox} , and substrate resistance, R_{si}, as well.

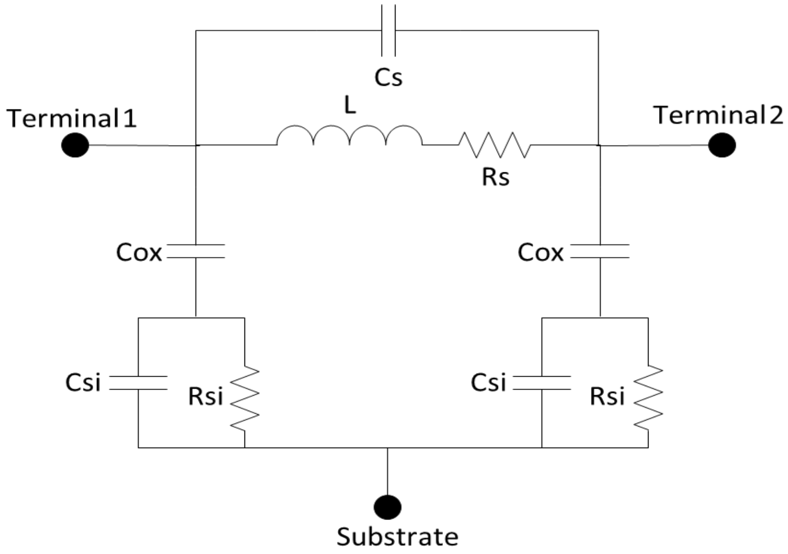

Fig. 5.6. πcircuit model of the spiral inductor.

The initial approach in the layout environment was the attempt to shrink the size of the inductor as much as possible to meet the required frequency of operation. Accordingly, the diameters (inner and outer) are selected in micro-meter range and by optimizing the parameters of the spiral inductor the following values were chosen, $n = 4$ which represents the number of turns of the hexagonal inductor. $d_{in} = 50\ \mu m$ and $d_{out} = 145\ \mu m$ are selected respectively. These values will result in $\rho = 0.49$ and $d_{avg} = 97.5\ \mu m$. Also $S = 2.5\ \mu m$ and $W = 7.5\ \mu m$ were chosen. By performing the frequency-based simulation the inductance of 2.6 nH was obtained as displayed in figure 5.7. It can be seen from the frequency sweep that the inductance value is in the range of 2.5 to 2.7 nano-Henry. This slight inductance variation is in the acceptable tolerance range.

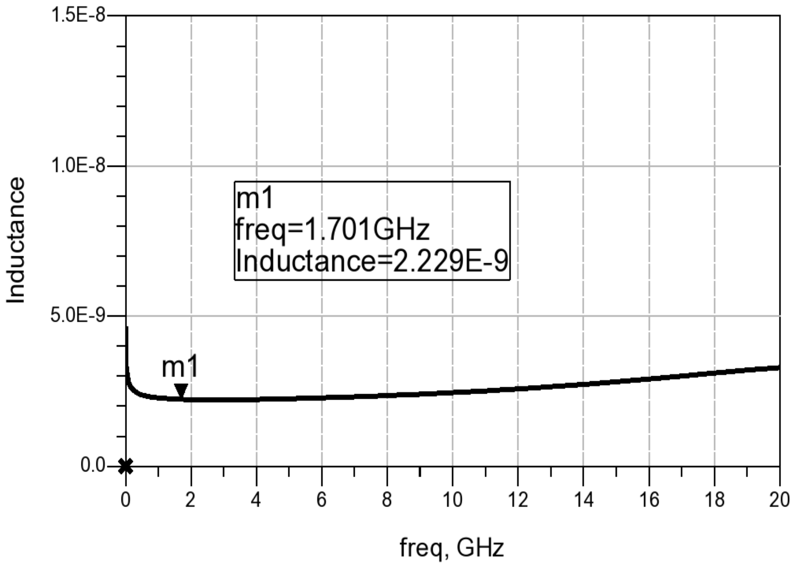

Figure 5.7 Inductance graph of the hexagonal inductor with respect to frequency sweep.

SIMULATION RESULTS

To test the validity of the presented method, a MEMS comb-drive was designed and simulated using Agilent's Advanced Design System (ADS). The 3D representation of the implemented comb-drive in figure5.8 (a) was used to perform the circuit level simulations. Figure5.8 (b) shows the same comb-drive with missing fingers which is used to observe the variations of the resonance frequency due to the physical defects.

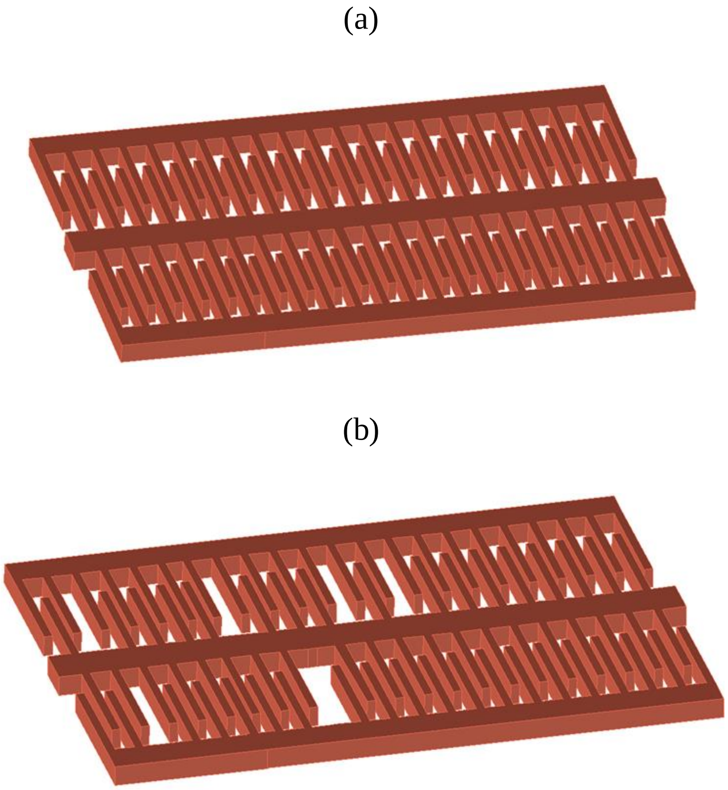

Fig 5.8 (a) Implemented comb-drive used to evaluate the proposed test method. (b) Comb-drive with missing fingers used for fault analysis.

Figure 5.9 presents the comb-drive MEMS structure in Coventorware environment after applying the stimulus. It can be seen that the stimulated movable arm deflects by as much as 10nm. This displacement affects the MEMS nominal capacitance and consequently the resonant frequency in the test mode.

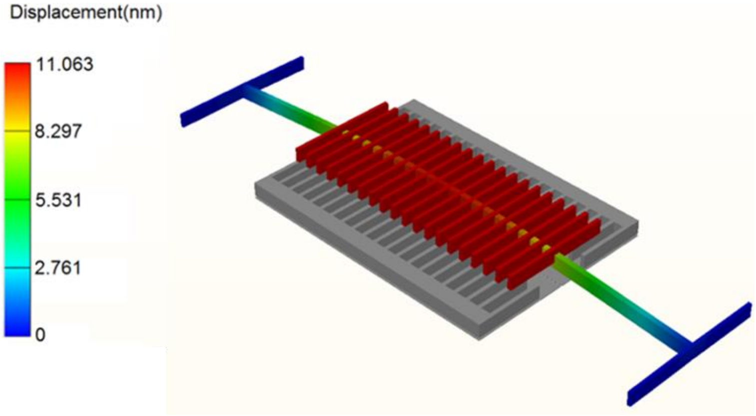

Fig. 5.9. Implemented capacitive MEMS and relevant arm deflection according to applying the stimulus.

The nominal capacitance of the structure that was obtained is shown in figure5.10 which remains in the range of 1.2 to 1.5 pico-Farad up to frequency of 5.0 GHz. At higher frequencies the capacitance increases due to the high frequency effects of the substrate used to implement the comb-drive.

After designing the spiral inductor and comb-drive separately, the next step was to do the analysis for both of them on the same chip. The internal impedance of the input port was selected to be 50 ohms for proper load matching. The generated layout of interconnects for the inductor and the comb-drive are displayed in figure 5.11.

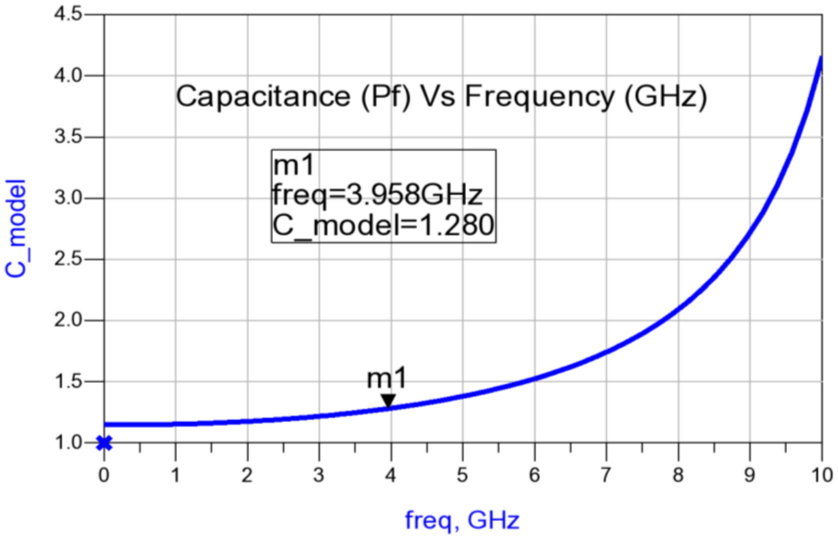

Fig. 5.10 Plot of the capacitance with respect to frequency sweep.

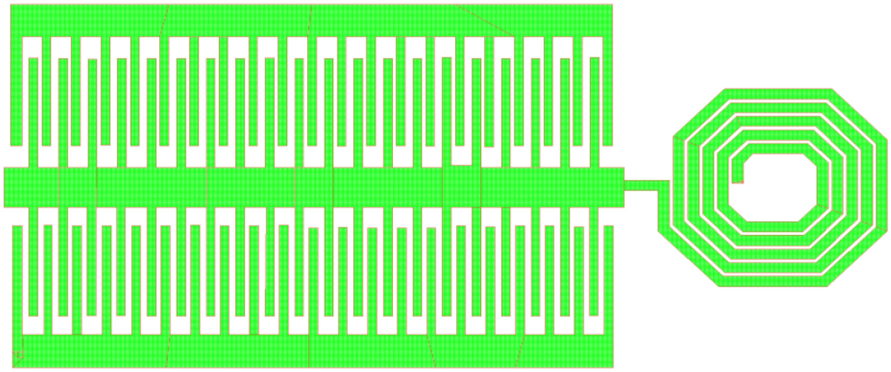

Fig. 5.11 Series combination of the comb-drive and spiral inductor.

The test circuit is designed to ensure that the resonance frequency falls below 5.0 GHz to avoid the undesired effects on the test results at higher frequencies. The test circuit was simulated using ADS and the output signal is shown in figure 5. 12. It can be seen that the output signal falls sharply at the resonance frequency of 3.958 GHz. From the resonant frequency for fault free device the capacitance of the comb-drive at the resonant frequency was determined to be 1.28 pF. This value was used as the reference capacitance in the test mode.

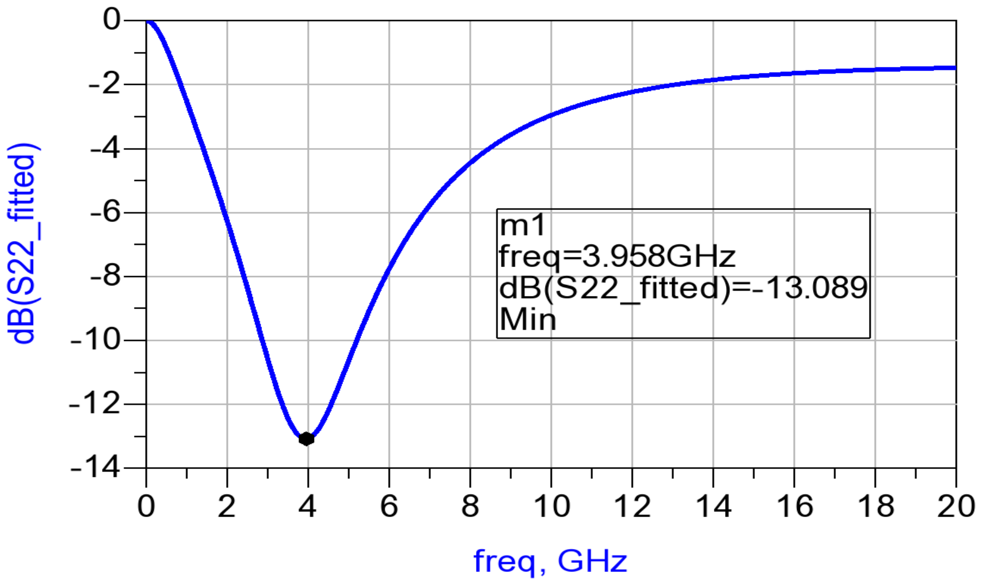

Fig. 5.12 Insertion loss of the circuit indicating that the inductance and the MEMS capacitance resonate at 3.958 GHz.

The effects of missing fingers on the MEMS capacitance and resonance frequency as part of structural defects have been summarized in Table I. The variations of the resonance frequency is linear and as the number of missing fingers increases as expected the capacitance decreases and the resonance frequency rises. It is also shown that the structural defects such as missing fingers will shift the frequency slightly. The frequency and the amplitude shifting are shown in figure5.13. It is noticeable that with each missing finger the amplitude of the signal increases respectively. The purple wave in figure 5.13 demonstrates the fault free case, light blue is the response for a case with a pair of missing fingers, the response of four pairs of missing fingers is presented by pink and ultimately the blue color displays the amplitude variations when there was six missing fingers. It can be observed that the amplitude variations with respect to the missing fingers increase. The variation of the resonant frequency with missing figures is summarized in Table. I.

TABLE I.VARIATIONS OF PERFORMANCE PARAMETERS OF THE IMPLEMENTED COMB DRIVEF WITH MISSING FINGERS.

Number of missing fingers	Total Capacitance (pF)	ΔC (fF)	f_{res} (GHz)	Δf_{res} (MHz)
0	1.280	0	3.958	0
2	1.272	8	3.974	16
4	1.263	17	3.995	37
6	1.254	26	4.022	64
8	1.247	33	4.031	73
10	1.239	41	4.063	107
12	1.225	55	4.088	130
14	1.216	64	4.117	159

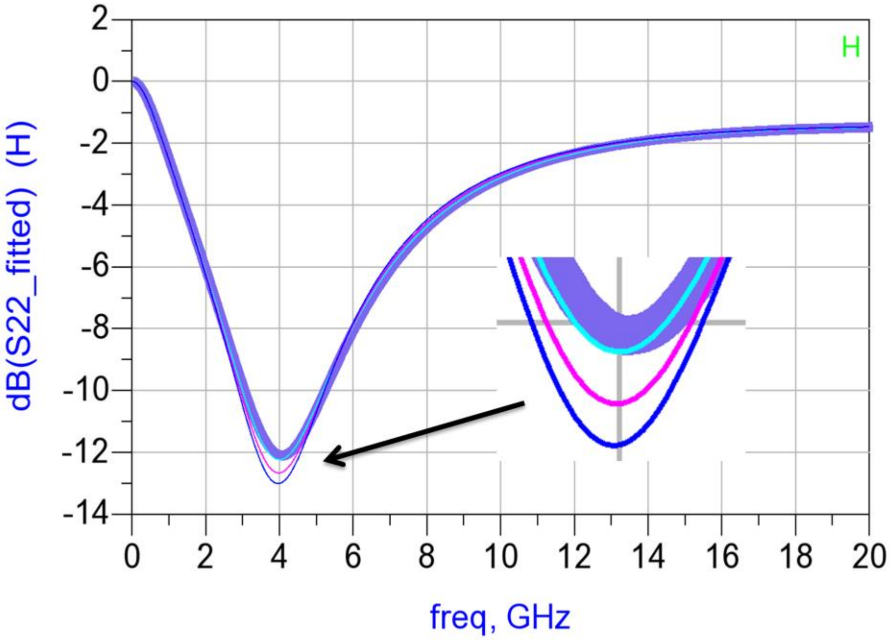

Fig. 5.13 S-parameter of the resonance circuit with respect to comb-drive missing fingers

The variation of output with respect to the frequency sweep for short fingers and tilted movable arm is shown in Table II. Simulations were also performed to see the effect of a high Q inductor on the output amplitude variations. The results indicate that the amplitude of the output signal varies approximately 1.0 dB from the reference value for each missing finger when an inductor with $Q = 40$ is used.

TABLE II.VARIATIONS OF PERFORMANCE PARAMETERS OF THE IMPLEMENTED COMB DRIVEF WITH SHORT FINGERS AND TILTED MOVABLE ARM.

	Output at the resonant frequency(dB)	f_{res} (GHz)	Δf_{res} (MHz)
Short fingers	-13.045	3.988	30
Tilted movable arm by 3 degrees	-19.765	4.019	61

Fabrication procedure and measurement results

In order to verify the validity of the proposed test solution, a comb-drive and a spiral inductor were fabricated using poly-MUMPs surface micromachining process. Poly-MUMPs technology is a three-layer poly-silicon surface micromachining process which is based on the silicon-on-insulator process. This process has the specific features as standard surface micromachining process.

According to Poly-MUMPs technology for structural material, silicon is used as the main material for the substrate. In the deposition stage an oxide of poly-silicon is deposited which is used as a sacrificial layer. For electrical isolation between the substrate and the poly-silicon, silicon nitride is used to create a three-layer poly structure that is needed to complete the poly-MUMPs material selection. The process commences first by doping the silicon wafer substrate heavily with phosphorus. This greatly helps to avoid the electrostatic charge between the surface and the substrate during fabrication process. In general, seven layers are used at the end of the fabrication phase which three of them are poly0; poly1 and poly2.There are also two poly’s oxides (1st and 2nd) layers and at the top and bottom of the structure as well as metal and nitride layers. The Poly-MUMPs fabrication process including the seven layers is represented in figure 5.14 [28].

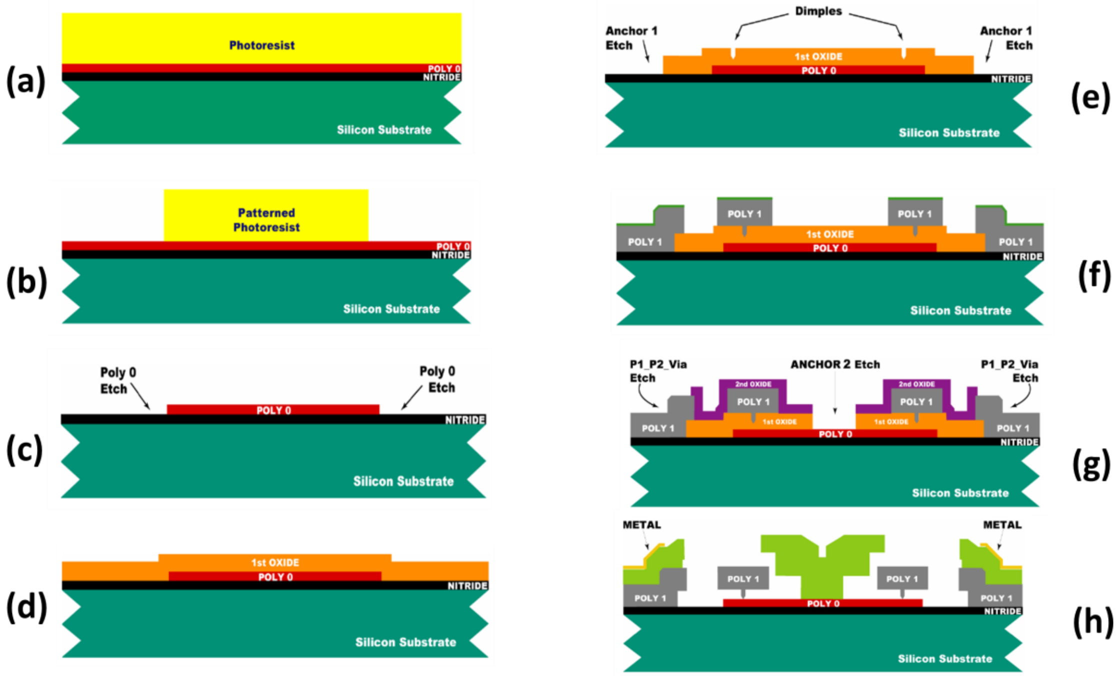

Figure 5.14 the Poly-MUMPs fabrication process[28].

Figure 5.14 (a) displays the silicon as substrate, Nitride, Poly0 and photo-resist as initial layers to begin the fabrication process. The photo-resist is used to coat wafers and also to assist the photolithography process. By developing the exposed photo-resist, it is possible to make a desired mask to transfer the pattern into the subsequent underlying layer as shown in figure5.14(b) and figure 5.14(c) where Poly0 is etched through plasma etch system. Next step is the deposition of phosphosilicate glass (PSG) also known as 1st oxide that is sacrificial layer with the thickness of 2 μm by low pressure chemical vapor deposition (LPCVD) process as shown in figure 5.14(d). This sacrificial layer is patterned lithographically with specific mask known as Dimple which is removed at the end of the process in order to free the first mechanical component of the poly-silicon. In order to create a hard mask for the next poly-silicon etch the PSG layer is etched initially There is a third mask layer called Anchor1 which is used to pattern the wafer again and also to reactivate the ion etch as demonstrated in figure 5.14(e). After the poly-silicon etch is done, the photo-resist is stripped and then the hard mask oxide is removed as shown in figure 5.14 (f). Next step is patterning the second oxide. This task is performed with two different etch masks to provide a connection between Poly1 and Poly2 electrically and mechanically. These two layers are lithographically patterned and etched. Anchor2 is another mask layer that is introduced to etch the first and the second oxide layers in a single step. This can assist in reducing misalignment between individual etched holes and also eliminating the need to make a cut in the oxides. This process is demonstrated in figure 5.14 (g) which includes the cross section of the wafer after completion of Poly1, Poly2 and Anchor2 levels. The final stage is the deposition and patterning of 0.5 μm of metal layer which is used in many applications such as probing, bonding and electrical routing. In this work, the metal is used to probe the spiral inductor. Figure5.14 (h) presents the final structure that needs to be immersed in de-ionized (DI) water and alcohol for at least 10 minutes in temperature of $110\ °C$respectively to reduce the stiction [28, 29]. The fabricated spiral inductor as well as probing station is presented in figure 5.15.

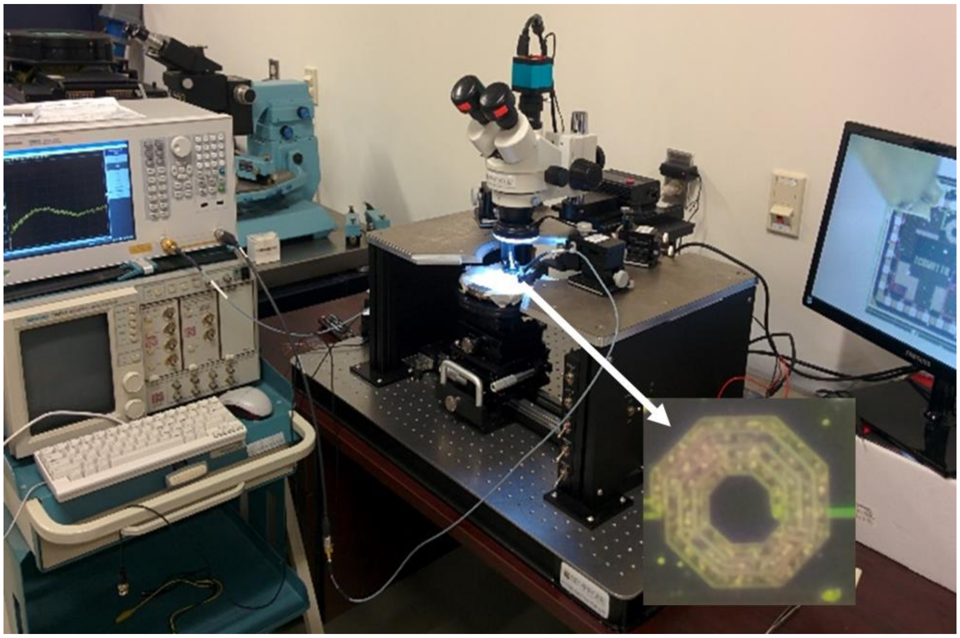

Figure 5.15 fabricated spiral inductor through Poly-MUMPs.

In order to measure the return loss of the resonant circuit, Agilent's E5016B network analyzer was used. The measurement results are shown in Fig. 5.16.

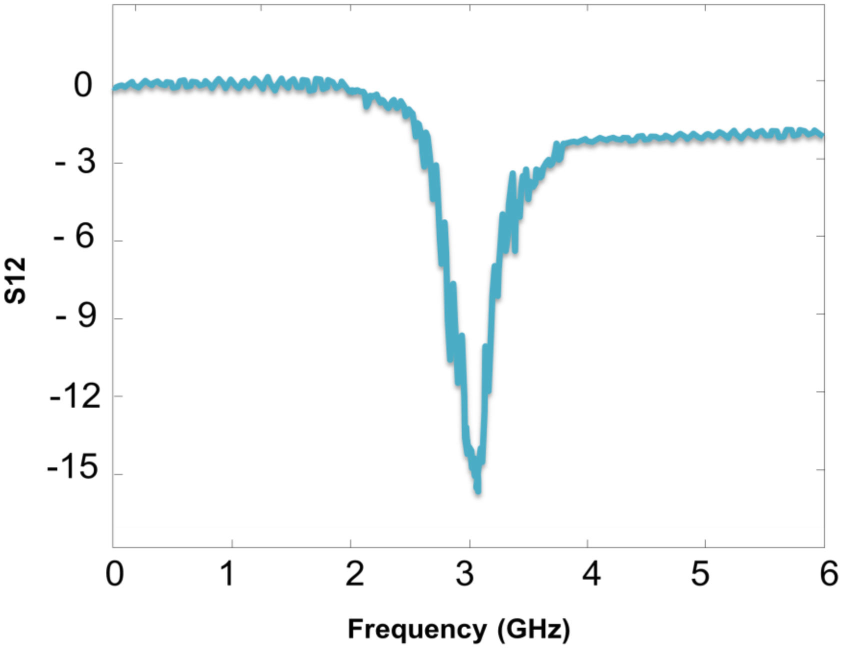

Fig. 5.16Obtained S-parameter of the resonance circuit

It can be seen that the resonance frequency drops sharply at 3.122 GHz which is close to the results obtained by simulation. The experimental measurements indicate that the proposed test solution could successfully detect broken, missing and shorted fingers.

Chapter 6

CONCLUSION

A test solution for capacitive MEMS presented in this work in which the test results are evaluated in the frequency domain rather than the time domain. It is shown that the frequency domain analysis has the potential to detect minor MEMS structural defects. Variations of the resonant frequency or the output amplitude can be observed to detect possible structural defects. Simulation results using an implemented comb-drive indicate that the presented test scheme can be utilized to detect missing fingers, short fingers and tilted arms. In the second phase of the work, an oscillator-based test solution for capacitive MEMS is presented in which the test results are inspected in frequency domain. Variations of the resonant frequency or the output amplitude can be observed to detect possible structural defects. Analytical analysis shows the proposed approach has the potential to detect minor MEMS structural defects. Variations in the output voltage swing and the resonance frequency alterations can be observed to detect possible structural defects.

Simulation results and experimental measurements using an implemented spiral inductor and a comb-drive indicate that the presented test scheme can be utilized to detect missing fingers, short fingers, broken and tilted arms in MEMS devices. The proposed method is easy to implement and has a high sensitivity to capture structural defects affecting the capacitance of MEMS sensors.

References

[1] StephenD. Senturia, “Microsystem Design”, Massachusetts Institute of Technology, KLUWER ACADEMIC PUBLISHERS, 2001,p. 3. ISBN0-306-47601-0.

[2]PRIME Faraday Partnership, “An introduction to MEMS”, Wolfson School of Mechanical and Manufacturing Engineering, Loughborough University, Prime Faraday Technology Watch, 2002 Loughborough University, p. 2, ISBN1-84402-020-7.

[3]SMi Pressure Sensors, “MEMS Pressure Sensor Solutions for Automotive Applications”, October 2013.

[4] Z. Gong, “TSVEquivalent Circuit Model using 3D Full-Wave Analysis”, MASc thesis, University of Windsor, Fall 2014.

[5] LIGA-Micro-machined gear for a mini electromagnetic motor, “HISTORY OF MICROELECTROMECHANICAL SYSTEMS (MEMS)”, Southwest Center for Microsystems Education and The Regents of University of New Mexico, Southwest Center for Microsystems Education (SCME), February 2001.

[6] Iantao Pan, “MEMS and Reliability”, Dependable Embedded Systems, Carnegie Mellon University, Spring 1999.

[7] S. Chowdhury, “A typical MEMS sensor and actuator systems,” electrical and computer engineering department lecture notes, University of Windsor, Winter 2013.

[8] J. Christophe Eloy, Yole Development, March 2011.

[9] Akustica company, “ AKU340 analog MEMS capacitive sensor microphone”, March 2011.

[10] W. Kern and C. A. Deckert, “Chemical etching,” in Thin Film Processes (J. L. ossen and W. Kern, eds.), pp. 401–496, New York: Academic Press, 1978.

[11] K. R. Williams and R. S. Muller, “Etch rates for micromachining processing,”Microelectromechanical Systems, vol. 5, pp. 256–269, 1996. The tables of data from this paper are also available at the web site of the Berkeley Sensors and Actuators Center.

[12] G. T. A. Kovacs, N. I. Maluf, and K. E. Petersen, “Bulk micromachining of silicon,” Proc. IEEE, vol. 86, pp. 1536–1551, 1998.

[13] C. Hedlund, U. Lindberg, U. Bucht, and J. Soderkvist, “Anisotropic etching of Z-cut quartz,” J. Micromechanics and Microeng.,vol. 3, pp. 65–73, 1993.

[14] P. B. Chu, J. T. Chen, R. Yeh, G. Lin, J. C. P. Huang, B. A. Warneke, and K. S. J. Pister, “Controlled pulse-etching with xenon diflouride,” in Proc.1997 Int’l. Conf. Solid-State Sensors and Actuators (TRANSDUCERS‘97), (Chicago), pp. 665–668, June 1997.

[15] S. A. Campbell, The Science and Engineering of Microelectronic Fabrication. New York: Oxford University Press, 1996.

[16] S. Wolf and R. N. Tauber, Silicon Processing for the VLSI Era, vol. 1: Process Technology. Sunset Beach, CA, USA: Lattice Press, second edition, 2000.

[17] M. Madou, Fundamentals of Microfabrication. New York: CRC Press, 1997.

[18] J. M. Bustillo, R. T. Howe, and R. S. Muller, “Surface micromachining for microelectromechanical systems,” Proc. IEEE, vol. 86, pp. 1552–1574,1998.

[19] M. A. Schmidt, R. T. Howe, S. D. Senturia, and J. H. Haritonidis, “Design and calibration of a microfabricated floating-element shearstress sensor,” IEEE Trans. Elec. Dev., vol. 35, pp. 750–757, 1988.

[20] P. F. Van Kessel, L. J. Hornbeck, R. E. Meier, and M. R. Douglass, “A MEMS-based projection display,” Proc. IEEE, vol. 98, pp. 1687–1704, 1998.

[21] Mark Burns, Gordon W. Roberts, “An Introduction to Mixed-Signal IC Test and Measurement,” New York Oxford, Oxford University Press, 2001,ISBN 0-19-514016-8.

[22] L. Rufer, S. Mir, E. Simeu, C. Domingues, "On-chip testing of MEMS using pseudo-random test sequences", Design, Test, Integration and Packaging of MEMS/MOEMS 2003. Symposium on, vol., no., pp.50, 55, 5-7 May 2003.

[23] J. Mizsei, M. Reggente, "MEMS Testing by Vibrating Capacitor", Design and Diagnostics of Electronic Circuits and Systems (DDECS), 2007 IEEE, vol., no., pp.1, 4, 11-13 April 2007.

[24] L. Ciganda, P. Bernardi, M.S. Reorda, D. Barbieri, M. Straiotto, L. Bonaria, "A tester architecture suitable for MEMS calibration and testing", Test Conference (ITC), 2010 IEEE International , vol., no., pp.1,1, 2-4 Nov. 2010.

[25] A. Rekik, F. Azais, N. Dumas, F. Mailly, P. Nouet, "Investigations on electrical-only test setup for MEMS convective accelerometer", Signals, Circuits and Systems (SCS), 2009 3rd International Conference on , vol., no., pp.1,6, 6-8 Nov. 2009.

[26] V. Litovski, M. Andrejevic, M. Zwolinski, "Behavioural modelling, simulation, test and diagnosis of MEMS using ANNs", Circuits and Systems (ISCAS), 2005 IEEE International Symposium on, vol., no., pp.5182, 5185 Vol. 5, 23-26 May 2005.

[27] S. Yanghe, Z. Honghai, W. Xuefang, L. Sheng, "A Base Exciter for Dynamic Testing of MEMS on Wafer Level", Electronic Packaging Technology (ICEPT), 2006 7th International Conference on, vol., no., pp.1, 3, 26-29 Aug. 2006.

[28] F. Oesterle, R. Weigel, A. Koelpin, "A new approach on MEMS sensor batch testing using an analogue parallel test methodology for massive reduction of test time", SENSORS, 2013 IEEE, vol., no., pp.1, 4, 3-6 Nov. 2013.

[29] N. Deb, R.D. Blanton, “Built-in selftest of CMOS-MEMS accelerometers”, Proceedings of International Test Conference, 2002, pp. 1075-1084.

[30] L. La Spina,N. Nenadovic, A.W. Van Herwaarden, H. Schellevis, W.H.A. Wien, L.K. Nanver, “MEMS test structure for measuring thermal conductivity of thin films”, IEEE International Conference on Microelectronic Test Structures ICMTS 2006, March 2006, pp. 137-142.

[31] P.M. Osterberg, S.D. Senturia, “M-TEST: A test chip for MEMS material property measurement using electrostatically actuated test structures”, Journal of Microelectromechanical Systems, vol. 6, no. 2, pp. 107-118, June 1997.

[32] A. Sisto, O. Schwarzelbach, L. Fanucci, “Fully electrical test procedure for inertial MEMS characterization at wafer-level”, 9th Conference on Ph.D. Research in Microelectronics and Electronics (PRIME), June 2013, pp. 121-124.

[33]X. Xiong, Y. Wu, W. Jone, "A dual-mode built-in self-test technique for capacitive MEMS devices", IEEE Transactions on Instrumentation and Measurement, vol. 54, no. 5, pp. 1739,1750, Oct. 2005.

[34]V. Natarajan, S. Bhattacharya, A. Chatterjee, “Alternate electrical tests for extracting mechanical parameters of MEMS accelerometer sensors”, Proceedings of IEEE VLSI Test Symposium, May 2006, pp. 6-10.

[35] B. Charlot, S. Mir, F. Parrain, B. Courtois, “Electrically induced stimuli for MEMS self-test”, 19th IEEE Proceedings on VLSI Test Symposium, VTS, 2001, pp. 210-215.

[36] A. Kansal, E.H. Sarraf, M. Sharma, E. Cretu, “Novel Adaptive FPGA-based Self-Calibration and Self-Testing Scheme with PN Sequences for MEMS-based Inertial Sensors”, IEEE 17th International Mixed-Signals, Sensors and Systems Test Workshop (IMS3TW), May 2011 pp. 120-126.

[37] T.M. Supon, K. Thangarajah, R. Rashidzadeh, M. Ahmadi, “A PLL based readout and built-in self-test for MEMS sensors” Circuits and Systems, IEEE 54th International Midwest Symposium, Aug. 2011, pp. 1-4.

[38] A.A. Rekik, F. Azais, F. Mailly, P. Nouet, M. Masmoudi, “Self-test and self-calibration of a MEMS convective accelerometer”, Symposium on Design, Test, Integration and Packaging of MEMS/MOEMS (DTIP), April 2013, pp. 1-4.

[39] A. Jain, S. Palit, M.A. Alam, “A Physics-Based Predictive Modeling Framework for Dielectric Charging and Creep in RF MEMS Capacitive Switches and Varactors”, Journal of Microelectromechanical Systems, vol. 21, no. 2, pp. 420-430, April 2012.

[40] X. Xingguo, Y.L. Wu, W.B. Jone, “A dual-mode built-in self-test technique for capacitive MEMS devices”, IEEE Transactions on Instrumentation and Measurement, vol. 54, no. 5, pp. 1739-1750, Oct. 2005.

[41] H. Thomas Lee, “The design of CMOS radio frequency integrated circuit”, Second edition, Cambridge university press, 2004, pp.632-633.

[42] Salmon, L.G., "Testing requirements for micro electromechanical systems (MEMS)," AUTOTESTCON '98. IEEE Systems Readiness Technology Conference., 1998 IEEE , vol., no., pp.160,, 24-27 Aug 1998, doi: 10.1109/AUTEST.1998.713436.

[43] Solanki, A.; Prasad, K.; Oreilly, R.; Singhal, Y., "Inertial MEMS Test Challenges," Mixed-Signals, Sensors and Systems Test Workshop (IMS3TW), 2011 IEEE 17thInternational , vol., no., pp.114,119, 16-18 May 2011 doi: 10.1109/IMS3TW.2011.12.

VITA AUCTORIS

NAME: Ali Dianat
PLACE OF BIRTH: Dezfoul, Khoozestan, Iran

YEAR OF BIRTH: 1985

EDUCATION: Shahed High School, Kermanshah, Kermanshah, Iran, 2003

University of Kermanshah, B.Eng. , Kermanshah, Iran, 2008
University of Windsor, Honor Certificate, Windsor, ON, Canada, 2011
University of Windsor, M.Eng., Windsor, ON, Canada, 2013
University of Windsor, M.A.Sc., Windsor, ON, Canada, 2015